Palaeolimnology of Lake Sapanca and identification of historic earthquake signals, Northern Anatolian Fault Zone (Turkey)

Markus J. Schwab*[a,b], Petra Werner*[a,c], Peter Dulski[b], Edward McGee[d], Norbert R. Nowaczyk[b], Sébastien Bertrand[a,e], Suzanne A.G. Leroy[a]

[a] Department of Geography and Earth Sciences and Institute for the Environment, Brunel University, Uxbridge, Middlesex UB8 3PH, London, UK.

[b] GFZ - German Research Centre For Geosciences, Section 3.3 Climate Dynamics and Sediments, Telegrafenberg, 14473 Potsdam, Germany

[c] Universität Osnabrück, FG Geographie, Seminarstraße 19a/b, 49069 Osnabrück, Germany

[d] Environmental Radiation Research Laboratory, Dept of Experimental Physics, University College, Dublin 4, Ireland

[e] Woods Hole Oceanographic Institution, Woods Hole, MA 02543, USA

*both authors have contributed equally to this paper and are corresponding authors;

Emails: M.J. Schwab: mschwab@gfz-potsdam.de, P. Werner: pw_bln@yahoo.com

Abstract

Lake Sapanca is located on a strand of the Northern Anatolian Fault Zone (NAFZ, Turkey), where a series of strong earthquakes (Ms > 6.0) have occurred over the past hundred years. Identifying prehistoric earthquakes in and around Lake Sapanca is key to a the better understanding of plate movements along the NAFZ. This study contributes to the development of palaeolimnological tools to identify past earthquakes in Lake Sapanca. To this end several promising proxies were investigated, specifically lithology, magnetic susceptibility, grain size (thin-section and laser analysis), geochemistry, pollen concentration, diatom assemblages, ^{137}Cs and ^{210}Pb. Sedimentological indicators provided evidence for reworked, turbidite-like or homogeneous facies (event layers) in several short cores (< 45 cm). Other indicators of sediment input and the historical chronicles available for the area suggest that three of these event layers likely originated from the AD 1957, 1967 and 1999 earthquakes. Recent changes in sediment deposition and nutrient levels have also been identified, but are probably not related to earthquakes. This study demonstrates that a combination of indicators can be used to recognize earthquake-related event layers in cores that encompass a longer period of time.

Keywords: natural hazards, historic earthquakes, multi-proxy approach, lacustrine sediments, Northern Anatolian Fault, Lake Sapanca

1 Introduction

Movements of the Anatolian and the Eurasian Plates along the Northern Anatolian Fault Zone (NAFZ) in western Turkey have led to several large earthquakes during the 20th century. Epicentres of large earthquakes have moved westward along the NAFZ towards the megacity of Istanbul (Barka, 1997; Stein et al., 1997). Reconstructing the history of past earthquakes contributes to better predicting future earthquakes in the region. Knowledge of past earthquakes in earthquake-prone areas raises the possibility of protecting humans and infrastructure (Atakan, et al., 2002; Sørensen et al., 2006). It was for these reasons that the European Union project on "Large Earthquake Faulting and Implications for the Seismic Hazard Assessment in Europe" (RELIEF) was initiated (Pantosti et al., 2008).

Lake Sapanca is an ideal study site, because the lake is located directly above the NAFZ fault at the centre of the RELIEF project region. Palaeoseismological trenches to the east and west of Lake Sapanca have provided evidence for palaeo-earthquakes (Rathje et al., 2000; Hitchcock et al., 2003; Altunel et al., 2004). However, it is important to complement trench investigations with a palaeolimnological study to provide a more complete picture of plate movements along the NAFZ, because movements along one part of the NAFZ may influence movements elsewhere (Lettis et al., 2002). Lake sediments may also contain an archive of past earthquakes, because they are deposited continuously.

Some researchers have successfully identified earthquakes using sedimentology, geochemistry, pollen or diatoms in lake sediments as proxy indicators (Sims, 1975; Ken-Tor et al., 2001; Arnaud et al., 2002). For example, sedimentology has been used to identify *in situ* deformations (Enzel et al., 2000; Becker et al., 2002; Migowski et al., 2004) and turbidite or homogenite deposits (Monecke et al., 2004; Bertrand et al.,

2008) generated by earthquakes. Similarly, earthquake-induced slumping and deposition of turbidites have been identified in lacustrine sediments of Lake Annecy, France (Beck et al., 1996), Lake Biwa, Japan (Inouchi et al., 1996) and Lake Le Bourget, France (Chapron et al., 1999). Geochemistry may indicate whether sediments are allochthonous or autochthonous and thus provide insights into earthquake-related changes in transport and sedimentation processes. The combination of sedimentological and geochemical indicators allows varying environmental changes to be better defined. For example, total organic carbon provides information about organic productivity within the lake, which mainly depends on primary productivity, and about productivity within the catchment (Wagner et al., 2004). Autochthonous organic carbon in a lake varies with changing vegetation cover in the catchment and changing precipitation patterns, which in turn may change vegetation cover and also sediment transport energy (Håkanson and Jansson, 1983; Wagner et al., 2004). In addition, the amount of total inorganic carbon, and changes in element composition, grain size, and magnetic susceptibility can be used as indicators of past environmental changes and earthquakes (Bertrand et al., 2005; Franz et al., 2006). Each lake reacts differently to strong earthquakes, due to its unique bathymetry and catchment characteristics (Becker et al., 2002). Specific earthquake signals first should be identified on short lake sediment cores that span a period with known earthquakes. This information can then be used to infer the earthquake history from long cores spanning thousands of years (e.g. Leroy et al., 2009 b).

Pollen have also been shown to record past earthquakes (Cowan and McGlone, 1991). For example, uplift or subsidence (Mathewes and Clague, 1994; Mirecki, 1996), or exposure of new habitat for pioneer plants (Cowan and McGlone, 1991)

may be evident in fossil pollen records in tectonically active areas. However, the NAFZ at Lake Sapanca is mostly a right-lateral strike-slip fault (Straub et al., 1997), and no extensive areas of uplift, subsidence or exposure of the fault plane would be expected in an earthquake. Therefore, in Lake Sapanca palynological data may provide indirect evidence of earthquakes, largely as a proxy for changes in sediment sources and sedimentation rates. For example, pollen concentrations may indicate whether sediment originated from rapid in-wash of soil, which are usually aerobic and pollen-barren, or by direct accumulation of pollen in deep water sediments, which are often anaerobic and pollen-rich.

Diatoms have been used successfully as palaeo-indicators of earthquakes in coastal waters (Hayward et al., 2004) and are potentially useful in lakes. Seepage of hydrothermal fluids along a fault located below the sea may lead to salinity or pH changes in the water during or after an earthquake (Claesson et al., 2004; Kuşçu et al., 2005). However, the local hydrogeological setting determines whether any change occurs at all (Sneed et al., 2003; Woith et al., 2003). For example, the 1999 earthquakes in northwest Turkey (Fig. 1) changed the conductivity of water in a well ~1400 km away from the epicentre. However, conductivity levels did not change in wells ~300-1200 km from the epicentre, due to differences in geology (Woith et al., 2003) and it is not known whether the water chemistry of Lake Sapanca changed during these earthquakes. Another possible earthquake-related limnological change in Lake Sapanca is an increase in nutrient levels caused by mobilisation of nutrients from sediments in the lake or its catchment. Diatoms are generally good palaeo-indicators of water chemistry changes (Stoermer and Smol, 1999) and can be used to identify whether the waters of Lake Sapanca changed following earthquakes.

The aim of this study is to test whether recent sediments deposited in Lake Sapanca contain proxy indicators of earthquakes over the past few thousands of years. Lithology, grain size (thin-section and laser analysis), magnetic susceptibility, geochemistry, pollen concentration, and diatom assemblages were studied for their ability to identify palaeo-earthquakes in Lake Sapanca.

2 The Study Site

Lake Sapanca is located ~90 km east of Istanbul in a tectonic pull-apart basin (Fig. 1). One of the strands of the western Northern Anatolian Fault Zone crosses the lake with an east-west orientation (Fig. 2). The NAFZ has an average slip rate of 1.5 cm/yr per year (Straub et al., 1997). Over the past century, the fault has produced five major (Ms 6.5-7.4) earthquakes: Hendek-Adazaparı (1943), Abant (1957), Mudurnu Valley (1967), Izmit (1999) and Düzce (1999) (Ambraseys, 2002; Ambraseys and Finkel, 1991), each of which potentially affected sedimentation and water quality in Lake Sapanca (Fig. 1; Lettis et al., 2002). Position FIGURE 1

The lake has a surface area of 46.8 km², a maximum depth of 55 m and stretches 16 km in an East-West direction and 5 km in a South-North direction (Albay et al. 2003; Fig. 2). The whole water column of Lake Sapanca mixes once a year in February-March, i.e. Lake Sapanca is a warm monomictic freshwater lake (Morkoç et al., 1998). Between 1989 and 1995 the pH levels of the lake ranged from 7.5 to 8.3 (Morkoç et al., 1998); total epilimnetic phosphorus levels ranged from 18.6 µg/l to 38.5 µg/l (Morkoç et al., 1998) and total epilimnetic nitrogen from 203 µg/l to 1,117 µg/l (Baykal et al., 1996). Position FIGURE 2

The area of the Lake Sapanca catchment is 251 km² (Fig. 1c). Steep slopes south of the lake rise to peaks up to ~1650 m asl. The area north of the lake is hilly with a

maximum elevation of ~350 m asl (Gürbüz and Gürer, 2008). Bedrock in the Lake Sapanca catchment includes schist, marble and metabasite south of the lake, andesite and basalt northeast and northwest of the lake, and sandstones and limestones (Ternek, 1964; Gürbüz and Gürer, 2008).

The vegetation around Lake Sapanca is part of the Euxinian domain, a temperate mixed forest ecoregion along the southern shore of the Black Sea (Quézel and Barbero, 1985). One-third of the lake's catchment is used for agriculture (33 %), 12 % is urban, industrial or other development; and forests and meadows constitute the remainder of the catchment (Baykal et al., 1996).

Annual mean air temperature and precipitation at Adapazarı (Fig. 1) over the past 30 years are 13°C and 830 mm, respectively. Storms with more than 80 mm of precipitation per day occurred on 3 July 1981 (88 mm), 30 July 1984 (82 mm) and 26 June 1999 (128 mm)(Devlet Meteoroloji Isleri Genel Mudurlugu, General Directorate of State Meteorological Works, Turkey). These early summer precipitation events are not known to have had any major effect on the stability of the lake shorelines. The mountain ranges south of Lake Sapanca receive much higher precipitation than the rest of the catchment. Fifteen small streams (Fig. 1C), which can dry up during summer and often have low sediment loads, provide the inflow to Lake Sapanca (Gürbüz and Gürer, 2008). The lake discharges through the canalised Çark River at the northeast end of the lake (Akkoyunlu and Ileri, 2003) (Fig. 2).

3 Methods

3.1 Coring and sedimentology

A Kajak gravity corer was used to retrieve 6-cm-diameter sediment cores up to 45 cm long in water depths of 23.5-54 m in 2003. Two cores were collected at each of

seven sites (K1 to K7) along two transects to identify events that affected the entire lake: across the fault and in the deep lake basin south of the fault (Fig. 2). This paper focuses on cores from the deep transect, i.e. cores K6.2 (40°43'05"N; 30°15'30"E; 53 m depth; core length 35 cm), K7.1 (40°43'05"N; 30°16'05"E; 54 m depth; core length 40 cm) and K7.2 (40°43'05"N; 30°16'05"E; 54 m depth; core length 34 cm).

Detailed lithological descriptions including Munsell soil colour and magnetic susceptibility, were done on all 14 cores. Other work included smear slide analyses (core K7.2), thin-section microscopy for grain size (core K7.1), laser particle-size analyses (cores K7.1 and 7.2) and water content (core K7.2). Sample thickness is reported in Table 1. Detailed sedimentary properties were determined with thin-section microscopy. A Malvern Mastersizer 2000 laser diffraction particle analyser was used to measure grain size in a composite profile from cores K7.2 (33-10 cm) and K7.1 (10-0 cm) at the University of Liège (Belgium), following the protocols of Bertrand et al. (2008) and using lithology and high-resolution magnetic susceptibility for correlating cores. Grain size statistics were calculated according to Folk and Ward (1957). Water content was determined by drying sediments at 105°C. Magnetic susceptibility was measured with a Bartington MS2E/1 spot-reading sensor following the 'split-core logging' method of Nowaczyk (2001). Position TABLE 1

3.2 Geochemistry

Total Carbon (TC) and Total Organic Carbon (TOC) were determined using a LECO carbon analyzer. The dried sediment samples were pulverised and homogenised. Sub-samples were treated with H_3PO_4 (1:1) to remove inorganic carbon prior to instrument analyses.

Major and minor elements were semi-quantitatively determined using Micro-X-Ray fluorescence spectrometry (µ-XRF) with the high-resolution core scanner EAGLE III BKA (Röntgenanalytik Messtechnik GmbH, Germany) (Table 1). Major components of the system are a Rh-X-Ray tube, a capillary lens system to focus the X-ray beam onto the sample surface and a Si(Li) semi-conductor detector. The space between the sample surface and Be-window of the detector is flushed with He (flow rate ~3.5 l/h) to minimize strong absorption of low-energy X-rays from lighter elements such as Al and Si. Elements were measured using a X-ray beam spot size of 250 µm, enlarged to 650 µm (3 x 3 raster) with 20 data points/cm. The resulting data are element intensities in counts per second (cps). Due to the dependence of the element response on, for example, the energy of fluorescence radiation, penetration depth, and matrix composition, intensity ratios differ significantly from concentration ratios. Because of the current calibration of the µ-XRF scanner, it was not feasible to normalize the elements by Al.

3.3 Pollen concentration

0.4-1 ml of sediment were subsampled from core K7.1 for palynological analysis (Table 1). Subsamples were successively treated with $Na_4P_2O_7$, HCl, HF and HCl, and then sieved through 125 and 10 µm screens. Numbers of microfossils per ml of wet sediment were calculated with the initial addition of *Lycopodium* tablets. Pollen residues were mounted in glycerol. Palynomorphs were identified at magnifications of 400x (routinely) and 1000x (special identification). All terrestrial and aquatic pollen grains and spores were included in determining concentrations. However, non–pollen and spore palynomorphs (mostly plankton and benthos) were excluded.

3.4 Diatoms

Diatoms in core K7.1 were processed and identified following standard procedures (Battarbee et al., 2001; Table 1). Samples were dried at 60 °C, treated with 30 % H_2O_2 and 10 % HCl and rinsed using centrifugation (5 min at 1200 rpm). Divinylbenzene microspheres were added, and residues were mounted using Naphrax®. A minimum of 300 valves per sample were counted under 1000x magnification unless diatom abundance was very low. In the latter case a minimum of 300 microspheres were counted and individual valves encountered in the count were specified. Taxonomy was based on Krammer and Lange-Bertalot (1986-1991). Biostratigraphic zones were identified with taxa present at least once at = 1% using Detrended Correspondence Analysis performed with the program CANOCO.

3.5 ^{137}Cs and ^{210}Pb

Cores K6.2 and K7.2 were dated using ^{137}Cs (Table 1; Appleby, 2001). ^{210}Pb stratigraphy was used to complement sedimentology. Sediment samples were dried at 60 °C for ~36 hours and then pulverised. ^{210}Pb, ^{214}Pb, ^{214}Bi, and ^{137}Cs activities were measured with high-resolution gamma spectrometry using an intrinsic n-type germanium detector. Supported ^{210}Pb in each sample was estimated using the average of ^{214}Bi and ^{214}Pb.

Deviation of excess ^{210}Pb activities from the characteristic logarithmic decay curve were used to identify variable sedimentation rates or non-chronological sedimentation, which would be expected for event deposits. The assumptions of commonly used ^{210}Pb age models were not fulfilled in this earthquake-prone area. For example, the constant initial concentration model and the constant rate of supply

model both require a constant pattern of sediment focussing (Appleby, 2001). Thus, core dating was mainly based on ^{137}Cs chronology.

4 Results

4.1 Sedimentology

All 14 cores consist mainly of relatively homogenous, black (2.5Y2/0), dark olive grey (5Y 3/2), or dark reddish brown (2.5YR 2.5/3) clayey-silt. The sequences include thin, discontinuous layers and lenses of silty clay, silt, and minor sandy-silt (Figs. 3 and 4). Thin-section (cores K6.2 and K7.1) and laser particle-size analysis (core K7.2) showed that the sediment consists dominantly of fine silt- and clay-sized particles; the mean grain size is in the range 5-11 µm (average 7.7 µm) (Figs. 3 and 4). In core K7.2 sand content is low (0.5-1.6 %), except at 6.5-2.5 cm, where the sand content is up to 3.0 % (Fig. 3). This sandy bed fines upward (Figs. 3 and 4). Above 2.5 cm the sand content is low (~0.5-1.7 %), but it increases again in the surface sample (2.4 %). Position FIGURE 3, Position FIGURE 4

Figure 4 provides a summary of lithofacies in cores K6.2 and K7.1 based on micro-facies and visual analyses. Four lithofacies are recognized:

1. U = undisturbed lacustrine facies; partly laminated clayey silt that was laid down in chronological order. In contrast, the remaining facies (R, T and H) present event layers.
2. R = reworked facies; clayey silt with some sand and visible terrestrial plant remains and a few small broken shell fragments. This lithofacies is present in core K7.1 (R_2, 28.0-23.8 cm; R_1, 23.25-19.5 cm) and core K6.2 (29.0-27.5 cm and 14.6-10.75 cm; the latter correlates to R_2 and R_1 in core K7.1) (Figs. 3 and 4).

3. T = turbidite-like facies; fining-upward sequence with a relatively sharp sandy base, clayey top and localized plant remains; present in core K7.1 as three thick layers (T_4, 37.5-32.5 cm; T_2, 19.5-16.0 cm; and T_1, 6.2-2.5 cm) and one thin layer (T_3, 23.8-23.25 cm), and in core K6.2 as two layers (T_4, 27.5-25.5 cm; and T_1, 3.25-2.0 cm). Layers T_2 and T_3 are not present in core K6.2, but they correlate by magnetic susceptibility to the reworked layer at 14.6-10.75 cm in that core.
4. H = homogeneous facies; non-graded, unlaminated silty clay; present only in core K7.1 (12.25-8.25 cm; corresponds to ~12.7-~8.3 cm in core K7.2), in which it is clearly distinct from the adjacent undisturbed lacustrine sediment (Figs. 3 and 4).

The words “turbidite” and “homogeneous” are used in the sense of Friedman and Sanders (1978) and Sturm et al. (1995). For small, confined lacustrine basins, they define a “homogenite” as fine-grained sediment that originates near the shore and slides towards the lake centre, where it is deposited under an oscillating current (seiche).

The water content ranges in core K7.2 from 40 to 72 % (average 55 %) (Fig. 3). The surface sediment has the highest water content; sediments at the base of the core and at 19.4 cm have the lowest water contents.

Magnetic susceptibility (MS) values range from 81×10^{-6}SI (core K7.2 at 6.8 cm) to 1093×10^{-6}SI (core K7.1 at 22.8 cm). MS varies significantly through each core (changes $>10\times10^{-6}$SI), allowing correlations to be made among cores (Figs. 3 and 5). Most cores exhibit one dominant susceptibility peak, which provides an excellent marker horizon – the maximum at 13.7 cm in core K6.2 correlates with those at 22.8 cm in core K7.1 and 20.4 cm in core K7.2 (Fig. 5). Generally, MS values are higher in the lower parts of cores (e.g., in core K7.1 $>180\times10^{-6}$SI from 37 to 15 cm, but $<180\times10^{-6}$SI from 15 to 1 cm) (Fig. 3 and 5). Position FIGURE 5

4.2 Geochemistry

In core K7.2 total carbon (TC) ranges from 1.3 to 4 weight % (standard deviation ±0.02 %) (Fig. 3). TC comprises approximately equal amounts of total inorganic carbon (TIC, range 0.4-2.0 %) and total organic carbon (TOC, 0.9-2.8 ± 0.05 %). Overall, trends of TIC, TOC and TC through the core are similar and are positively correlated to water content (R^2=0.63; Fig. 3). Values of all three variables are relatively low in lower sediments (TC = 1.3-2.5 % at 34.0-14.5 cm) and are higher in upper sediments (TC = 2.7-4.2 % at 14.5-0 cm). An exception is lower TC from 4.6 to 2.1 cm (2.3-2.7 %).

µ-XRF scanning of core K7.1 allowed clastic (Al, Si, K, Ti and Fe), diagenetic (Fe) and biogenic (Ca) signals to be recognized (Fig. 6; Rollingson, 1995; Eusterhues et al., 2002; Vlag et al., 2004). Down-core variations in Al intensities are positively correlated with Si, K and Ti, and several trends are evident through core K7.2. At the base of the turbidite-like layer at 37.5 cm (T_4), Al, Si, K and Ti values (= clastic indicators) increase abruptly and reach maxima (Fig. 6). The clastic indicators decrease upward, with a brief peak at the small T-facies layer (T_3) at 23.25 cm and an abrupt second maximum directly above layer R_1 at 19.5 cm. Intensities are relatively constant between 14.5 and 8 cm, including the H-facies (12.25-8.25 cm), with the exception of potassium. Above 8.25 cm clastic element intensities decrease to their core minima at 8-6.25 cm and 2.25-0 cm (U-facies). In T_1 (6.25-2.25 cm) between the U-facies, clastic element intensities are slightly higher and relatively uniform. Overall, with the exception of K, clastic element intensities are lower above ~14.5 cm than below (Fig. 6). Position FIGURE 6

Ca intensities are negatively correlated to clastic element intensities, whereas Fe intensities showed no linear relationship to the clastic indicators. Fe and Ca exhibit prominent maxima in layer R_1 at 23.25-20.25 cm. Al, Si, K and Ti intensities in this layer are low. Shell fragments are particularly abundant at 25-20 cm (Fig. 4). Fe and magnetic susceptibility are positively correlated at several depths, notable at about 34.5, 28.5, 23.5-13.5 and 2.5-0 cm. No correlation is evident at other levels, for example 24.5-23.5 and 13.5-2.5 cm (Fig. 6).

4.3 Pollen concentration

Pollen preservation is excellent. Most pollen is of terrestrial origin; aquatic pollen is typically less than 2%). Pollen concentrations in core K7.1 range from 2,900 grains/ml to 43,000 grains/ml (Fig. 6). Concentrations are low from 38.25 cm to 13.6 cm (<20,000 grains/ml), with minima at 37.1-35.1 and 23.1-17.1 cm, and high from 13.6 cm to 0 cm (mainly >20,000 grains/ml).

4.4 Diatoms

Core K7.1 can be divided into three diatom zones (DI-III) using Detrended Correspondence Analyses. Benthic taxa dominate (79-99 %) in Zone DI (26.25-7.5 cm), especially small benthic *Fragilaria* spp., but decrease to 4-15 % in Zone DII (7.5-2.75 cm) and DIII (2.75-0 cm) (Fig. 7). Benthic diatom concentrations, however, remain relatively constant throughout the core (0.1-3.4 frustules * 10^7/g). Position FIGURE 7

Zone DII is characterised by high relative abundances of planktonic *Fragilaria ulna* (var. *angustissima* and var. *acus*), *Stephanodiscus agassizensis* and *St. hantzschii,* and tychoplanktonic *Aulacoseira ambigua* (collectively 57-78 %; Fig. 7).

These taxa decrease to 23-52 % in Zone DIII, where they are replaced by the planktonic species *Cyclostephanos dubius*, *Cyclotella ocellata* and the benthic species *Cymbella microcephala* (together 25-54 % in DIII) (Fig. 7). Planktonic and tychoplanktonic diatom concentrations increase from Zone DI (0.0-0.1 frustules * 10^7/g) to Zone II and III (0.4-20.0 frustules * 10^7/g).

Diatom concentrations are very low (0.05-2.80 frustules * 10^7/g) in Zone DI. They increase to 6.7 frustules * 10^7/g at the base of Zone DII (6.75-6.50 cm), but subsequently decrease to 1.4-2.2 * 10^7/g frustules from 6.25 cm to 2.75 cm (Fig. 7). Concentrations are high in Zone DIII, ranging from 3.6 to 23.4 frustules * 10^7/g (Fig. 7).

4.5 ^{137}Cs and ^{210}Pb

Two ^{137}Cs peaks are present in both core K6.2 and core K7.2 (Fig. 8), facilitating correlation of the two. The deeper peaks (19-18 cm in core K6.2 and 32-31 cm in core K7.2) very likely represent 1963, the year of maximum fallout from the testing of nuclear weapons (Appleby, 2001). The second peaks (7-6 cm in core K6.2 and 13-12 cm in core K7.2) probably represent 1986, the year of the Chernobyl accident, which affected the study area (UNSCEAR, 1988; Karakelle et al., 2002; Kazancı et al., 2006). Position FIGURE 8

The unsupported ^{210}Pb profiles through cores K6.2 and K7.2 do not follow an exponential decline curve that is typical of ^{210}Pb, if the pattern of sediment focussing is constant (Fig. 8). Overall, ^{210}Pb levels are very low in sediments of H-, T- or R-facies in the two cores (Fig. 8).

5 Discussion

Palaeolimnological indicators suggest changing sedimentation processes, changing water chemistry and unusual disturbance events in Lake Sapanca over the past several decades.

5.1 Sedimentation processes

Differences between recent and older Lake Sapanca sediments indicate that sedimentation processes have changed in recent years. Most indicators change above ~14.5 cm in cores K7. Magnetic susceptibility and Si, Al, K, Ti intensities decrease, and total carbon, water content and pollen concentrations increase, above 14.5 cm (Fig. 9). These changes suggest lower input of allochthonous clastic material during deposition of the younger sediments.

The generally higher MS values in the lower parts of the cores can be explained by higher amounts of iron-rich sediment, lower amounts of autochthonous or allochthonous organic matter (Sangode et al., 2001; Geiss et al., 2003; Arnaud et al., 2005), or a change in grain size (Geiss et al., 2003). The lower overall levels of TIC, TOC and TC in the older sediments may partly explain the higher levels of MS. Additionally, water content is low where MS is high, suggesting a lower porosity and the possibility that pore space has been filled with Fe-rich silt and clay (Figs. 3 and 9). Diagenetic processes, such as precipitation of authigenic siderite ($FeCO_3$), can also increase MS. Siderite was observed microscopically throughout the cores (Fig. 4).

Infrastructure projects around Lake Sapanca may have contributed mineral dust and other sources of iron-rich and clastic sediments to the lake. Naturally, the entire catchment may also contribute clastic sediments to the lake (Gürbüz and Gürer, 2008). Additionally, there are three possible natural sources of iron-rich sediment

within the lake catchment. The first and greatest source is the rocks in the mountain range to the south, mainly schist, marble and metabasite. The other two sources are two small areas of andesitic and basaltic rock northeast and northwest of the lake (Ternek, 1964; Bakan, 1995). Changes in the delivery of sediment to the lake from the different source rocks may have led to a change in the iron content of the sediment.

The higher clastic element (Si, Al, K and Ti) intensities below 14.5 cm suggest greater allochthonous sediment input earlier relative to later. Al, Ti and K, are generally not involved in biogenic processes or precipitation/dissolution reactions, and are interpreted as indicators of allochthonous minerogenic detritus (Dean, 1993; Rollingson, 1995; Eusterhues et al., 2002; Vlag et al., 2004). Si intensities are strongly correlated with Al, Ti and K (Fig. 6) and therefore, probably also denote changes in allochthonous material input. Si of biogenic origin probably only contributes little to the total Si intensities, as the Si content and diatom concentration were hardly correlated with each other (Fig. 9). Clastic sediment enters Lake Sapanca via rivers, soil erosion by surface runoff and, to a lesser extent, by aeolian transport (Kubilay et al., 2001).

Pollen concentrations increase markedly above ~13.6 cm in core K7.1 (Fig. 9). Low pollen concentration may indicate that the sediment originated from areas in which pollen was oxidised (Bennett and Willis, 2001; Leroy et al., 2009 a). In Lake Sapanca, such areas include the shoreline and vegetated soils. The marked change in pollen concentrations in core K7.1 suggests that more allochthonous material was contributed to the older sediments.

The ^{137}Cs chronology indicates that the sediments below 14.5 cm were deposited within several decades prior to 1986 (Fig. 8). A likely explanation for the greater allochthonous material input below ~14.5 cm is major motorway and railway

construction projects that lasted for decades and ended in the early 1980s. A national road was built along the north shore of Lake Sapanca in the 1950s and a railway was built along the south shore in 1975. In addition, the Trans-European Motorway was constructed in the area in the 1980s (Yalçin and Sevinç, 2001), and dykes were built to regulate stream inflow during periods of high rainfall (Gürbüz and Gürer, 2008). Position FIGURE 9

5.2 Water chemistry

The ecologies of the important diatoms found in Lake Sapanca sediments (Gasse et al., 1995; Dixit et al., 1999) do not indicate any pH, conductivity or chloride level changes in Lake Sapanca over the past ~40 years. The diatom changes were likely due to changes in nutrient levels (Fig. 7). Diatom taxa dominating Zone DI require relatively low nutrient levels (Wunsam and Schmidt, 1995; Dixit et al., 1999). The dominant taxa in DII, *Aulacoseira ambigua*, *Fragilaria ulna* and *Stephanodiscus agassizensis*, require relatively high phosphate levels (Håkansson and Kling, 1989; Wunsam and Schmidt, 1995; Dixit et al., 1999; Rivera et al., 2002), and the dominant diatoms from Zone DIII (*Cyclostephanos dubius*, *Cyclotella ocellata*) suggest high to medium high nutrient levels (Bennion et al., 1996, Bradshaw et al., 2002).

Zone DI also has the lowest total diatom concentrations (Figs. 7 and 9), supporting the inference that nutrient levels were lowest in Zone DI. Similarly, concentrations of tychoplanktonic and planktonic diatom taxa increased significantly from Zone DI to Zone DII and DIII, whereas benthic diatom concentrations remained relatively constant throughout the core. These changes indicate that the lake waters were relative clear during Zone DI compared to Zones DII and DIII. An alternative explanation for the low phytoplankton concentrations concurrent with relatively

constant benthic diatom concentrations is that the diatoms in Zone DI originated from shallow waters that were diluted by allochthonous material.

Earthquakes may change nutrient levels, for example by sewage leakage or rapid inputs of nutrients from the catchment. However, most disturbance layers (T-, H-, and R-facies) do not coincide with changes in diatom composition or concentration, therefore the diatom-inferred nutrient level changes do not seem to be related to earthquakes (Fig. 9).

5.3 Disturbance events

Thin section microscopy shows that the cores consist of layers of undisturbed lacustrine sediment punctuated by event layers (Figs. 3, 4 and 9). These event layers include the reworked (R), turbidite-like (T) or homogeneous (H) lithofacies (Table 2). The most recent event (Event 1) is recorded by the turbidite-like layer T_1. Event 2 is marked by homogeneous layer H. Event 3 is recorded by reworked (R) and turbidite-like layers (T_2 and T_3). Event 4 is marked by turbidite-like layer T_4 in core K7.1 and the reworked layer in core K6.2 (Table 2).

The palaeo-indicators exhibit different signals at the event layers. Grain size, magnetic susceptibility, organic and inorganic carbon, Fe and Ca element intensities, pollen concentration and diatom assemblages and concentrations differ among events (Fig. 9). In contrast, clastic element intensities and ^{210}Pb activities do not differ significantly from event to event. For example, all T-facies layers, and especially their bases, are characterised by relatively high clastic element intensities (Si, Al, K and Ti). Coarse clastic input suggests a higher amount of allochthonous material in the T-facies compared to the other facies. Also, unusually low ^{210}Pb activities correspond to the event layers in cores K6.2 and K7.2 (Fig. 8). The low activities can not be fully

explained by errors inherent in the method. Instead, they could be due to older sediment being laid down on younger sediment or faster sediment accumulation than in the adjacent sediment layers (Appleby and Oldfield, 1983). Position TABLE 2

The T-, H- and R-facies layers could be caused by earthquake-induced slumps, non-seismic slope failures, or floods (Karlin and Abella, 1996; Eastwood et al., 1999). Lake levels have been monitored since 1955 and have remained constant at about 31-32 m asl, with intra-annual fluctuations of 1 m (EIEI 1999, 2002). They can thus be ruled out as a cause of the event sedimentation. A seismic origin is favoured by the correlation of events layers with large historical earthquakes (Migowski et al, 2004, Nomade et al., 2005; Bertrand et al., 2008).

Mobilisation, transport and deposition of sediment would be facilitated by the steep southern basin slope (Fig. 2) and may be responsible for the sedimentological differences among cores, such as the succession of T- and R-facies layers (R_2-T_3-R_1-T_2) from 28-16 cm in cores K7, which correlates to the R-facies layer in core K6.2 (14.6-10.75 cm) (Figs. 3, 4 and 5). The H-facies layer was identified in cores K7 (12.25-8.25 cm), but not in nearby core K6.2 (Fig. 4). Thus, the event responsible for the non-graded H-facies did not affect the entire lake basin. A local mass movement in Lake Sapanca closer to cores K7 than cores K6 could have affected only core site K7.

The topmost T_1-facies layer **(Event 1)**, is present in three cores (K6.2, K7.1 and K7.2), suggesting that it was a lake-wide event. The fining-upward sequence, coarse sediment grains at the base, low and constant diatom concentrations and homogeneous diatom assemblages through several centimetres of sediment suggest that this layer was deposited quickly. High levels of Al, Si, K and Ti and relatively

low diatom concentrations suggest that the material mainly originated from allochthonous sources.

Diatom-Zone DII (7.5-2.75 cm) includes this T_1-facies (6.3-2.5 cm). It shows little change in the diatom assemblages and relatively low and constant diatom concentrations compared to adjacent sediment layers (Figs. 8 and 9). The diatom results suggest sediment mixing or rapid sedimentation, weeks rather than years. Diatoms respond within days to changing environmental conditions, therefore each 0.25 cm of sediment deposited at normal rates will show minor changes in the diatom assemblages. If, however, the sediment accumulated relatively quickly, the diatom assemblages of several adjacent samples in a core might be relatively homogeneous.

The ^{137}Cs chronology suggests that the T_1-facies layer was deposited after 1986 (Fig. 8). Thus, Event 1 could be the 1999 Izmit/Düzce earthquakes (Table 2). The 1999 Izmit earthquake (Ms 7.4) caused extensive ground deformation along the shoreline of Lake Sapanca, especially near the town of Sapanca (Cetin et al., 2002; Lettis et al., 2002; Atak et al., 2004). Liquefaction and subsidence of the river delta were observed at the Sapanca Hotel along the southern shore, close to cores K6 and K7 (Fig. 2), and lateral spread of the southern shore was also observed (Bardet et al., 2000; Cetin et al., 2002).

The heavy rainfall event in 1999 could have contributed sediment to the event layer. This event produced more rainfall (128 mm) than the two other strongest storms of the past 30 years - 88 mm in one day in 1981, and 82 mm in one day in 1984 (data from DMI), and it is the only one that can be linked chronologically to an event layer. However, the amount of sediment delivered during the 1999 storm was probably small, because the inflowing streams were dammed (Gürbüz and Gürer, 2008).

The homogeneous H-facies (**Event 2**) is only present in cores from site K7. Homogeneous sediments can be derived from earthquake-induced water oscillations in lakes, which lead to resuspension of fine-grained sediments, as for example in Lake Le Bourget (Chapron et al., 1999), Lake Lucerne (Siegenthaler et al., 1987; Schnellmann et al., 2002) and Lake Icalma (Bertrand et al., 2008). Liquefaction-induced ground deformations are known to have occurred along the shoreline of Lake Sapanca, especially near the town of Sapanca (Cetin et al., 2002; Lettis et al., 2002; Atak et al., 2004). However, the H-facies bed is located just above the 1986 ^{137}Cs peak and thus probably is only a little younger than 1986 (Fig. 8). Event 2 thus does not correlate with either the 1967 or 1999 major earthquakes. Smaller earthquakes (Ms < 6.5) may have disturbed Lake Sapanca at this time (Ambraseys, 2002), but none of the indicators suggests that Event 2 is a lake-wide event. Also, there is no evidence for soil inwash, which might be expected during an earthquake. Thus, the origin of this event layer remains unknown (Table 2).

Event 3 is recorded in K6.2, K7.1 and K7.2: as a R-facies layer in core K6.2 and as a succession of T- and R-facies (R_2-T_3-R_1-T_2) in cores K7.1 and K7.2. The fining-upward sequence in T-facies layers indicates rapid sedimentation. The layers are characterised by high levels of Al, Si, K and Ti, which suggests high allochthonous clastic input. Similarly, high MS (maximum values in almost all of the 14 cores) and Fe in the R_1-facies layer are also most likely due to input of allochthonous sediment and indicate that Event 3 probably affected a large area of the lake. Macrophytic remains, reworked shells and high TC and Ca contents suggest that the R_1- and R_2-facies originated in shallow water. Thus, the sediments of Event 3 may be a mixture of shallow water and allochthonous terrestrial clastic sediments. This origin is supported by an abrupt decrease of pollen concentrations (increased aerobic pollen

exposure) between the R_2-T_3-facies and the R_1-T_2-facies, which suggests that the sediments of R_2 and T_3 are of different origin from the sediments of R_1 and T_2 (Fig. 9).

The MS maximum in Lake Sapanca, which corresponds to the R-facies in core K6.2 and the R_1-facies in cores K7 (Figs. 3 and 4), is probably due to increased input of allochthonous iron-rich material. Diagenetic processes within the sediments, such as precipitation of authigenic siderite, can also elevate MS, but cannot explain the MS maximum, because siderite grains were not visible in thin-sections at the depth of the MS maximum in cores K7.1 and K6.2 (Fig. 4). The temporal and spatial continuity of MS peaks in the Lake Sapanca cores and coincident changes in sedimentology are strong evidence for lake-wide events (Fig. 5; Sims, 1975; Nikonov, 1995).

The R_1 layer in cores K7 (23.25-19.5 cm) corresponds to a slight increase in TC (Figs. 3 and 9). TIC is probably closely linked to shell fragments and TOC to terrestrial plant material. Both of these components are visible in the R_1 layer thin-sections (Fig. 4). Therefore, the increase in TC in the R_1-layer in cores K7 suggests that the sediment originated close to the shore.

Ca content is influenced by organic productivity and detrital input (Figs. 4, 6 and 7). Ca intensities are high in the shell-rich parts of the R_1-facies layer in core K7.1 (23.25-19.5 cm). This Ca maximum coincides with the MS and Fe peaks (Fig. 6). Therefore, these R_1-sediments (23.25-19.5 cm) likely originated in shallow waters. They may have been delivered to the deeper lake basin by liquefaction, seismic seiches, slumps or turbidites.

The R-facies in core K6.2 (14.6-10.75 cm) and the T/R-facies in core K7.2 **(**29.2-16.7 cm**)** are located between the two ^{137}Cs peaks (1963 and 1986) and therefore may be related to the 1967 Mudurnu Valley earthquake or the 1981/1984 heavy

precipitation events (Fig. 8). These event layers are more likely associated with the 1967 earthquake, because they lie closer to the 1963 peak than the 1986 peak. Additionally, inflowing streams were dammed in the 1970s, thus the heavy precipitation events in 1981 and 1984 are unlikely to have contributed sediment to the event layer. The 1967 earthquake (Ms 7.1) had an epicentre 40 km from Sapanca and produced liquefaction at the southern shore of the lake, subsidence of the river delta, ground failure and building damage around the lake (Ambraseys and Zatopek, 1969; Bardet et al., 2000; Palyvos et al., 2007). Thus, we conclude that Event 3 most likely records the 1967 Mudurnu Valley earthquake (Table 2).

Event 4 is recorded in cores K6.2 (succession of T_4- and R-facies) and core K7.1 (T_4-facies). The event is probably located just below the bottom of core K7.2 (Fig. 9). High Al, Si, K, and Ti, especially at the T_4-facies base, and very low pollen concentrations again suggest high allochthonous clastic input. The fining-upward sequence suggests rapid sedimentation. The ^{137}Cs chronology suggests that Event 4 is older than 1963. Therefore, Event 4 may correspond to the Abant earthquake in 1957.

6 Conclusion

This study has identified several important events in the recent history of Lake Sapanca. Several indicators suggest a recent change (~1980-2003) in sedimentation processes, which may be due to constructions of roads and railroads over a period of several decades or, more likely, to constructions of dykes and dams in the 1970s to regulate inflow and outflow of Lake Sapanca. Several years after this shift in sedimentation, diatom assemblage changes suggest that nutrient levels increased markedly for some years before decreasing to still-higher-than background levels in the late 1990s.

Thin-section microscopy, grain size distributions, magnetic susceptibility, geochemical results, pollen concentrations, diatoms, ^{210}Pb and ^{137}Cs identified sedimentary events that likely correlate to the 1957, 1967 and 1999 earthquakes. Each proxy showed different signals in these event layers. Thus, only a combination of proxies will allow the identification of earthquakes over the past few thousands of years.

Acknowledgements

We are grateful to N. Hill (drilling, preliminary analyses), P. Costa, A. Holland, P. Szadorsky (advice and assistance in the laboratory), and M. Turner (editing of English) (Brunel University). The following persons provided help with field work, laboratory analyses and interpretation: M. Albay (Istanbul University), L. Doner (ITU Istanbul), M. Dreßler (University Rostock), S. Houghton (UCLondon), O. Ileri (MTA Ankara), S. Keogh (UCDublin), R. Klee (Bayerisches Landesamt für Wasserwirtschaft, Germany, *Stephanodiscus* spp. taxonomy), M. Köhler (GFZ), S. Öncel (Gebze Institute of Technology), H.-C. Treutler (UFZ, ^{210}Pb chronology interpretation), Ç. Yalçiner (Eskisehir University) and S. Boyraz (University of Ankara). G. Haug (GFZ) made magnetic susceptibility and µ-XRF measurements possible, and J. Thurow (UCL) facilitated carbon measurements. Additionally, we thank the reviewers and editors, who contributed considerably to the improvement of this manuscript. This study was funded by the EU as part of the EC Project RELIEF (EVG1-CT-2002-00069).

References

Akkoyunlu, A., Ileri, R., 2003. Evaluation of eutrophication process in Lake Sapanca (Sakarya, Turkey). International Journal of Environment and Pollution 19, 576-602.

Albay, M., Akçaalan, R., Tüfekçi, H., Metcalf, S.J., Beattie, A.K., Codd, A.G., 2003. Depth profiles of cyanobacterial hepatotoxins (microcystins) in three Turkish freshwater lakes. Hydrobiologia 505, 89-95.

Altunel, E., Meghraoui, M., Akyüz, S., Dikbas, A., 2004. Characteristics of the 1912 co-seismic rupture along the North Anatolian Fault Zone (Turkey): Implications for the expected Marmara earthquake. Terra Nova 16, 368-370.

Ambraseys, N.N., 2002. The seismic activity of the Marmara Sea region over the last 2000 years. Bulletin of the Seismological Society of America 92, 1-18.

Ambraseys, N.N., Zatopek, A., 1969. The Mudurnu Valley earthquake of July 22, 1967. Bulletin of the Seismological Society of America 59, 521-589.

Ambraseys, N.N., Finkel, C., 1991. Long term seismicity of Istanbul and of the Marmara Sea region. Terra Nova 3, 527-539.

Appleby, P.G., 2001. Chronostratigraphic techniques in recent sediments. In: Last, W.M., Smol, J.P. (Eds.), Tracking Environmental Change Using Lake Sediments. Vol. 1: Basin Analysis, Coring, and Chronological Techniques. Kluwer Academic Publishers, Dordrecht, pp. 171-203.

Appleby, P.G., Oldfield, F., 1983. The assessment of ^{210}Pb from sites with varying sediment accumulation rates. Hydrobiologia 103, 29-35.

Arnaud, F., Lignier, V., Revel, M., Desmet, M., Beck, C., Pourchet, M., Charlet, F., Trentesaux, A., Tribovillard, N., 2002. Flood and earthquake disturbance of ^{210}Pb geochronology (Lake Anterne, NW Alps). Terra Nova 14, 225-232.

Arnaud, F., Revel-Rolland, M., Chapron, E., Desmet, M., Tribovillard, N., 2005. 7200 years of Rhône river flooding activity in Lake Le Bourget: A high resolution sediment record of NW Alps hydrology. Holocene 15, 420-428.

Atak, V.O., Aksu, O., Aydan, Ö., Önder, M., Toz, G., 2004. Measurement of ground deformation induced by liquefaction and faulting in the 1999 Kocaeli earthquake area. XXth ISPRS Congress, Istanbul, Turkey, Commission VII papers, XXXV (B7), pp. 648-652.

Atakan, K., Ojeda, A., Meghraoui, M., Barka, A.A., Erdik, M., Bodare, A., 2002. Seismic hazard in Istanbul following the 17 August 1999 Izmit and 12 November 1999 Düzce earthquakes. Bulletin of the Seismological Society of America 92, 466-482.

Bakan, G., 1995. The study of the Sapanca lake ecosystem: Sediment characterisation and water quality modelling. Ph.D. thesis, Middle East Technical University, Ankara, Turkey (in Turkish).

Bardet, J.P., Cetin, K.O., Lettis, W., Rathje, E., Rau, G., Seed, R.B., Ural, D., 2000. Kocaeli, Turkey, earthquake of August 17, 1999: Reconnaissance report. Soil liquefaction, landslides and subsidences. Earthquake Spectra 16 A, 141-162.

Barka, A.A., 1997. Neotectonics of the Marmara region. In: Schindler, C., Pfister, M. (Eds.), Active Tectonics of Northwest Anatolia. The Marmara Poly-Project, Hochschulverlag AG ETHZ, Zürich, pp. 55-87.

Battarbee, R.W., Jones, V.J., Flower, R.J., Cameron, N.G., Bennion, H., Carvalho, L., Juggins, S., 2001. Diatoms. In: Smol, J.P., Birks, H.J.B., Last, W.M. (Eds.), Tracking Environmental Change Using Lake Sediments. Vol. 3, Terrestrial, Algal, and Siliceous Indicators. Kluwer Academic Publishers, Dordrecht, Boston, London, pp. 155-202.

Baykal, B.B., Gonenc, I.E., Meric, M., Tanik, A., Tunay, O., 1996. An alternative approach for evaluation of lake water quality: Lake Sapanca - A case study from Turkey. Water Science and Technology 34, 73-81.

Beck, C., Manalt, F., Chapron, E., van Rensbergen, P., De Batist, M., 1996. Enhanced seismicity in the Early post-glacial period: evidence from the post-Würm sediments of Lake Annecy, Northwestern Alps. Journal of Geodynamics 22, 155-171.

Becker, A., Davenport, C.A., Giardini, D., 2002. Earthquake scaling and the strength of seismogenic faults, Geophysical Journal International 149, 659-678.

Bennett, K.D., Willis, K.J., 2001. Pollen. In: Smol, J.P., Birks, H.J.B., Last, W.M. (Eds.), Tracking Environmental Change Using Lake Sediments. Vol. 3, Terrestrial, algal, and siliceous indicators. Kluwer Academic Publishers, Dordrecht, Boston, London, pp. 5-32.

Bennion, H., Juggins, S., Anderson, N.J., 1996. Predicting epilimnetic phosphorous concentrations using an improved diatom-based transfer function and its application to lake eutrophication management. Environmental Science & Technology 30, 2004-2007.

Bertrand, S., Boës, X., Castiaux, J., Charlet, F., Urrutia, F., Espinoza, C., Lepoint, G., Charlier, B., Fage, N., 2005. Temporal evolution of sediment supply in Lago Puyehue (Southern Chile) during the last 600 yr and its climatic significance. Quaternary Research 64, 163-175.

Bertrand, S., Charlet, F., Chapron, E., Fagel, N., De Batist, M., 2008. Reconstruction of the Holocene seismotectonic activity of the Southern Andes from seismites recorded in Lago Icalma, Chile, 39°S. Palaeogeography, Palaeoclimatology, Palaeoecology 259, 301-322.

Bradshaw, E.G., Anderson, N.J., Jensen, J.P., Jeppesen, E., 2002. Phosphorus dynamics in Danish lakes and the implications for diatom ecology and palaeoecology. Freshwater Biology 47, 1963-1975.

Cetin, K.O., Youd, L.L., Seed, R.B., Bray, J.D., Sancio, R., Lettis, W., Yilmaz, M.T., Durgunoglu, H.T., 2002. Liquefaction-induced ground deformations at Hotel Sapanca during Kocaeli (Izmit), Turkey earthquake. Soil Dynamics and Earthquake Engineering 22, 1083-1092.

Chapron, E., Beck, C., Pourchet, M., Deconink, J.F., 1999. 1822 earthquake-triggered homogenite in Lake Le Bourget (NW Alps). Terra Nova 11, 86-92.

Claesson, L., Skelton, A., Graham, C., Dietl, C., Mörth, M., Torssander, P., Kockum, I., 2004. Hydrogeochemical changes before and after a major earthquake. Geology 32, 641-644.

Cowan, H.A., McGlone, M.S., 1991. Late Holocene displacements and characteristic earthquakes on the Hope River segment of the Hope Fault, New Zealand. Journal of the Royal Society of New Zealand 21, 373-384.

Dean, W.E., 1993. Physical properties, mineralogy, and geochemistry of Holocene varved sediments from Elk Lake, Minnesota. In: Bradbury, J.P., Dean, W.E. (Eds.), Elk Lake, Minnesota: Evidence for Rapid Climate Change in the North-Central United States, Geological Society of America Special Paper 276, Boulder, pp. 135-157.

Dixit, S.S., Smol, J.P., Charles, D.F., Hughes, R.M., Paulsen, S.G., Collins, G.B., 1999. Assessing water quality changes in the lakes of the north-eastern United States using sediment diatoms. Canadian Journal of Fisheries and Aquatic Sciences 56, 131-152.

Eastwood, W.J., Roberts, N., Lamb, H.F., Tibby, J.C., 1999. Holocene environmental change in southwest Turkey: A palaeoecological record of lake and catchment-related changes. Quaternary Science Reviews 18, 671-695.

EIEI, 1999. Göl seviyeleri. Elektrik Isleri Etüt Idaresi Hidrolik Etütleri Dairesi, Ankara, Yayin no. 99-7 (in Turkish).

EIEI, 2002. Göl seviyeleri. Elektrik Isleri Etüt Idaresi Hidrolik Etütleri Dairesi, Ankara (in Turkish).

Enzel, Y., Kadan, G., Eyal, Y., 2000. Holocene earthquakes inferred from a fan-delta sequence in the Dead Sea graben. Quaternary Research 53, 34-48.

Eusterhues, K., Lechterbeck, J., Schneider, J., Wolf-Brozio, U., 2002. Late- and post-glacial evolution of Lake Steisslingen (I). Sedimentary history, palynological record and inorganic geochemical indicators. Palaeogeography, Palaeoclimatology, Palaeoecology 187, 341-371.

Folk, R.L., Ward, W.C., 1957. Brazos River bar: A study in the significance of grain size parameters. Journal of Sedimentary Petrology 27, 3-26.

Franz, S.O., Niessen, F., Schwark, L., Brüchmann, C., Scharf, B., Klingel, R., Van Alstine, J.D., Cagatay, M.N., Ülgen, U.B., 2006. Results from a multi-disciplinary sedimentary pilot study of tectonic Lake Iznik (NW Turkey) - Geochemistry and paleolimnology of the recent past. Journal of Paleolimnology 35, 715-736.

Friedman, G.M., Sanders, J.E., 1978. Principles of Sedimentology. John Wiley & Sons, New York.

Gasse, F., Juggins, S., Ben Khelifa, L., 1995. Diatom-based transfer function for inferring past hydrochemical characteristics of African lakes. Palaeogeography, Palaeoclimatology, Palaeoecology 117, 31-54.

Geiss, C.E., Umbanhowar, C.E., Camill, P., Banerjee, S.K., 2003. Sediment magnetic properties reveal Holocene climate change along the Minnesota prairie-forest ecotone. Journal of Paleolimnology 30, 151-166.

Gürbüz, A., Gürer, Ö.F., 2008. Anthropogenic affects on lake sedimentation process: a case study from Lake Sapanca, NW Turkey. Environmental Geology 56, 299-307.

Håkanson L., Jansson, M., 1983. Principles of Lake Sedimentology. Springer-Verlag, Berlin.

Håkansson, H., Kling, H., 1989. A light and electron microscope study of previously described and new *Stephanodiscus* species (Bacillariophyceae) from central and northern Canadian lakes, with ecological notes on the species. Diatom Research 4, 269-288.

Hayward, B.W., Cochran, U., Southall, K., Wiggins, E., Grenfell, H.R., Sabaa, A., Shane, P.R., Gehrels, R., 2004. Micropalaeontological evidence for the Holocene earthquake history of the eastern Bay of Plenty, New Zealand, and a new index for determining the land elevation record. Quaternary Science Reviews 23, 1651-1667.

Hitchcock, C., Altunel, E., Barka, A., Bachhuber, J., Lettis, W., Helms, J., Lindvall, S., 2003. Timing of late Holocene earthquakes on the Eastern Düzce Fault and implications for slip transfer between the southern and northern strands of the North Anatolian Fault System, Bolu, Turkey. Turkish Journal of Earth Sciences 12, 119-136.

Inouchi, Y., Kinugasa, Y., Kumon, F., Nakano, S., Yasumatsu, S., Shiki, T., 1996. Turbidites as records of intense palaeoearthquakes in Lake Biwa, Japan. Sedimentary Geology 104, 117-125.

Karakelle, B., Öztürk, N., Köse, A., Varinlioğlu, A., Erkol, A.Y., Yilmaz, F., 2002. Natural radioactivity in soil samples of Kocaeli basin, Turkey. Journal of Radioanalytical and Nuclear Chemistry 254, 649-651.

Karlin, R.E., Abella, S.E.B., 1996. A history of Pacific Northwest earthquakes recorded in Holocene sediments from Lake Washington. Journal of Geophysical Research 101, 6137-6150.

Kazancı, N., Toprak, Ö., Leroy, S.A.G., Öncel, S., Ileri, Ö., Emre, Ö., Costa, P., Erturaç, K., McGee, E., 2006. Boron content of Lake Ulubat sediment: A key to interpret the morphological history of NW Anatolia, Turkey. Applied Geochemistry 21, 134-151.

Ken-Tor, R., Enzel, Y., Stein, M., Marco, S., Negendank, J.F.W., 2001. High-resolution geological record of historic earthquakes in the Dead Sea basin. Journal of Geophysical Research 106, 2221-2234.

Krammer, K., Lange-Bertalot, H., 1986, 1988, 1991a, 1991b. Bacillariophyceae, 1-4. Teil. In: Ettle, H., Gerloff, J., Heynig, H., Mollenhauer, D. (Eds.), Süßwasserflora von Mitteleuropa, Band 2/1-4. Gustav Fischer Verlag, Stuttgart/Jena.

Kubilay, N., Nickovic, S., Moulin, C., Dulac, F., 2000. An illustration of the transport and deposition of mineral dust onto the eastern Mediterranean. Atmospheric Environment 34, 1293-1303.

Kuşçu, I., Okamura, M., Matsuoka, H., Gökaşan, E., Awata, Y., Tur, H., Şimşek, M., Keçer, M., 2005. Seafloor gas seeps and sediment failures triggered by the August 17, 1999 earthquake in the eastern part of the Gulf of İzmit, Sea of Marmara, NW Turkey. Marine Geology 215, 193-214.

Leroy, S.A.G., Boyraz, S., Gürbüz, A., 2009 a. High-resolution palynological analysis in Lake Sapanca as a tool to detect earthquakes on the North Anatolian Fault over

the last 55 years. In: Clague, J.J., Korup, O. (Eds.), Special Issue Quaternary Science Reviews. *This issue.*

Leroy, S.A.G., Schwab, M.J., Costa, P., 2009 b, accepted pending revisions. The tectonic influence on the last 1500-year infill history of a deep lake located on the North Anatolian Fault: Lake Sapanca (N-W Turkey). Quaternary Science Reviews.

Lettis, W., Bachhuber, J., Witter, R., Brankman, C., Randolph, C.E., Barka, A., Page, W.D., Kaya, A., 2002. Influence of releasing step-overs on surface fault rupture and fault segmentation: examples from the 17 August 1999 Izmit earthquake on the North Anatolian Fault, Turkey. Bulletin of the Seismological Society of America 92, 19-42.

Mathewes, R.W., Clague, J.J., 1994. Detection of large prehistoric earthquakes in the Pacific Northwest by microfossil analysis. Science 264, 688-691.

Migowski, C., Agnon, A., Bookman, R., Negendank, J.F.W., Stein, M., 2004. Recurrence pattern of Holocene earthquakes along the Dead Sea transform revealed by varve-counting and radiocarbon dating of lacustrine sediments. Earth and Planetary Science Letters 222, 301-314.

Mirecki, J.E., 1996. Recognition of the 1811-1812 new Madrid earthquakes in Reelfoot lake, Tennessee sediments using pollen data. Journal of Paleolimnology 15, 183-191.

Monecke, K., Anselmetti, F.S., Becker, A., Sturm, M., Giardini, D., 2004. The record of historic earthquakes in lake sediments of Central Switzerland. Tectonophysics 394, 21-40.

Morkoç, E., Tuğrul, S., Öztürk, M., Tufekçi, H., Egesel, L., Tüfekçi, V., Okay, O.S., Legović, T., 1998. Trophic characteristics of the Sapanca lake (Turkey). Croatica Chemica Acta 71, 303-322.

Nikonov, A.A., 1995. The stratigraphic method in the study of large past earthquakes. Quaternary International 25, 47-55.

Nomade, J., Chapron, E., Desmet, M., Reyss, J.L., Arnaud, F., Lignier, V., 2005. Reconstructing historical seismicity from lake sediments (Lake Laffrey, western Alps, France). Terra Nova 17, 350-357.

Nowaczyk, N.R., 2001. Logging of magnetic susceptibility. In: Last, W.M., Smol, J.P. (Eds.), Tracking Environmental Change Using Lake Sediments. Vol. 1: Basin Analyses, Coring, and Chronological Techniques. Kluwer Academic Publishers, Dordrecht, pp. 155-170.

Palyvos, N., Pantosti, D., Zabci, C., D'Addezio, G., 2007. Paleoseismological evidence of recent earthquakes on the Mudurnu Valley, 1967 earthquake segment of the North Anatolian Fault Zone. Bulletin of the Seismological Society of America 97, 1646 - 1661.

Pantosti, D., Pucci, S., Palyvos, N., De Martini, P.-M., D' Addezzio, G., Collins, P., Zabci, Z., 2008. Paleoearthquakes of the Düzce fault (North Anatolian Fault Zone): Insights for large surface faulting earthquake recurrence. Journal of Geophysical Research 113, B01309, 20 pp. doi:10.1029/2006JB004679.

Quézel, P., Barbero, M., 1985. Carte de la végétation potentielle de la région Méditerranéenne. Feuille 1: Mediterranée Orientale scale 1:2,500,000. Centre Nationale de la Recherche Scientifique (ed.), Paris, France.

Rathje, E., Idriss, I.M., Somerville, P., Ansal, A., Bachhuber, J., Baturay, M., Frost, D., Lettis, W., Sozer, B., Ugras, T., 2000. Kocaeli, Turkey, earthquake of August

17, 1999: Reconnaissance report. Strong ground motions and site effects, Earthquake Spectra 16 A, 65–96.

Rivera, P., Cruces, F., Vila, I., 2002. First record of *Stephanodiscus agassizensis* Hakansson and Kling (Bacillariophyceae) in Chile. Gayana Botánica 59, 79-86.

Rollingson, H., 1995. Using Geochemical Data: Evaluation, Presentation, Interpretation. Longman Group, Harlow.

Sangode, S., Suresh, J., Bagati, N., 2001. Godavari source in the Bengal fan sediments: Results from magnetic susceptibility dispersal pattern. Current Science 80, 660-664.

Schnellmann, M., Anselmetti, F.S., Giardini, D., McKenzie, J.A., Ward, S.N., 2002. Prehistoric earthquake history revealed by lacustrine slump deposits. Geology 30, 1131-1134.

Siegenthaler, C., Finger, W., Kelts, K., Wang, S., 1987. Earthquake and seiche deposits in Lake Lucerne, Switzerland. Eclogae Geologicae Helvetiae 80, 241-260.

Sims, J.D., 1975. Determining earthquake recurrence intervals from deformational structures in young lacustrine sediments. Tectonophysics 29, 141-152.

Sneed, M., Galloway, D.L., Cunningham, W.L., 2003. Earthquakes - rattling the Earth's plumbing system. U.S. Department of the Interior, U.S. Geological Survey. Fact Sheet 096-03.

Sørensen, M.B., Oprsal, I., Bonnefoy-Claudet, S., Atakan, K. Mai, M., Pulido, N. Yalciner, C., 2006. Local site effects in Atakoy, Istanbul, Turkey, due to a future large earthquake in the Marmara Sea. Geophysical Journal International 167, 1413-1424.

Stein, R.S., Barka A.A., Dieterich, J.H., 1997. Progressive failure on the North Anatolian Fault since 1939 earthquake stress triggering. Geophysical Journal International 128, 594-604.

Stoermer, E.F., Smol, J.P., 1999. The Diatoms: Applications for the Environmental and Earth Sciences. Cambridge University Press. Cambridge.

Straub, C., Kahle, H.-G., Schindler, C., 1997. GPS and geologic estimates of the tectonic activity in the Marmara Sea region, NW Anatolia, Journal of Geophysical Research 102, 27587-27602.

Sturm, M., Siegenthaler, C., Pickrill, R.A., 1995. Turbidites and 'homogenites'. A conceptual model of flood and slide deposits. International Association of Sedimentologists-16th Regional Meeting of Sedimentology, Publication ASF 22, Paris.

Tanik, A., Baykal, B.B., Gönenç, E., Meriç, S., Öktem, Y., 1998. Effect and control of pollution in catchment area of Lake Sapanca, Turkey. Environmental Mangement 22, 407-414.

Ternek, Z., 1964. Geologic map of Turkey, Istanbul, and Zonguldak sheets. Institute of Mineral Research and Exploration, Ankara, Turkey, scale 1:500,000.

UNSCEAR, 1988. Annex D: Exposures from the Chernobyl accident. In: United Nations Scientific Committee on the Effects of Atomic Radiation (UNSCEAR) 1988 Report to the General Assembly about the Sources, Effects and Risks of Ionizing Radiation, pp. 1-74.

Vlag, P.A., Kruiver, P.P., Dekkers, M.J., 2004. Evaluating climate change by multivariate statistical techniques on magnetic and chemical properties of marine sediments (Azores region). Palaeogeography, Palaeoclimatology, Palaeoecology 212, 23-44.

Wagner, B., Cremer, H., Hultzsch, N., Gore, D., Melles, M., 2004. Late Pleistocene and Holocene history of Lake Terrasovoje, Amery Oasis, East Antarctica, and its climatic and environmental implications. Journal of Paleolimnology 32, 321-339.

Woith, H., Wang, R., Milkereit, C., Zschau, J., Maiwald, U., Pekdeger, A., 2003. Heterogeneous response of hydrogeological systems to the Izmit and Düzce (Turkey) earthquakes of 1999. Hydrogeology Journal 11, 113-121.

Wunsam, S., Schmidt, R., 1995. A diatom-phosphorus transfer function for lakes of the Alps and pre-alpine region. Memorie dell Istituto di Idrobiologia 53, 85-99.

Yalçin, N., Sevinç, V., 2001. Heavy metal contents of Lake Sapanca. Turkish Journal of Chemistry 25, 521-525.

Figure captions

Fig. 1: A) Location of study area in northwestern Anatolia, Turkey. B) Tectonic setting of the Northern Anatolian Fault Zone (NAFZ). Stars indicate the epicentres of the Hendek-Adazaparı (1943), Abant (May 1957), Mudurnu (July 1967), Izmit (August 1999) and Düzce (November 1999) earthquakes. Modified from Hitchcock et al. (2003). C) Catchment of Lake Sapanca showing inflowing streams. Modified from Tanik et al. (1998); image NASA Landsat N-35-40-2000 https://zulu.ssc.nasa.gov.

Fig. 2: Bathymetric map of Lake Sapanca, showing core sites along the cross-fault transect (K1-5) and the deep transect (K5-7). Also shown is the trace of the Northern Anatolian Fault (NAF) (modified from Lettis et al., 2002).

Fig. 3: Lithology, grain size, lithofacies and magnetic susceptibility in cores K6.2, K7.1 and K7.2. Also shown is water content, organic matter (TOC), total carbon (TC) and total inorganic carbon (TIC) for core K7.2. Correlations between cores are based on lithology or colour (solid lines) and magnetic susceptibility (dashed lines). Grain size is based on thin-section microscopy in cores K6.2 and K7.1 and laser optical analyses from a composite profile of cores K7.2 (34-10 cm) and K7.1 (10-0 cm). Note the discontinuous x-axis for laser optical grain size.

Fig. 4: Lithology, core photographs and interpretation of cores K6.2 and K7.1 based on visual description and thin-section microscopy.

Fig. 5: Magnetic susceptibility [10^{-6} SI] and correlations between cores from an A) cross-fault transect and B) deep transect. Correlation is based on magnetic susceptibility and lithology (thin black dashed lines) or solely on magnetic susceptibility (thin grey dashed lines). Correlations of all cores are highlighted with a thick grey line. Ambiguous correlations are labelled with a question mark.

Fig. 6: Comparison of µ-XRF element intensities with sedimentology, magnetic susceptibility and pollen concentrations in core K7.1. Element intensities are given in counts per minute (cps). Grey horizontal layers are event layers (reworked, turbidite-like and homogeneous).

Fig. 7: Relative abundance of important diatoms (present in at least in one sample at 5%), diatom concentrations and relative abundance of planktonic (pl), tychoplanktonic (ty) and benthic (be) diatoms in core K7.1. Each row totals 100 % relative abundance. Solid bars indicate that at least 300 valves were counted. Numbers to the left of grey bars are total number of valves counted where less than 300. Small *Fragilaria* include mainly *Fragilaria brevistriata*, *F. construens* var. *venter*, *F. construens* var. *venter/construens*, *F. leptostauron dubia* and *F. pinnata*.

Fig. 8: Supported ^{210}Pb (^{214}Bi and ^{214}Pb), total ^{210}Pb, ^{137}Cs and unsupported ^{210}Pb ($^{210}Pb_{exess}$), ^{137}Cs (dark grey area), chronology derived from ^{137}Cs (1963 and 1986) and sedimentological interpretation (facies types; light grey horizontal bars) for cores A) K6.2 and B) K7.2. Solid black line = $^{210}Pb_{total}$ and $^{210}Pb_{exess}$. Note different depth scales for cores K6.2 and K7.2.

Fig. 9: Comparison of the main palaeo-indicators in core K7.1 (magnetic susceptibility, diatom-inferred (Di) nutrient levels, diatom concentration, silica, pollen concentration, facies interpretation) and core K7.2 (total carbon, mean grain size, excess ^{210}Pb and ^{137}Cs). Diatom zones (DI-DIII) correspond to DI-DIII in Fig. 7. Note reversed x-axis for pollen concentration. Event layers (E1-E4) are shown in grey across the cores. Correlations of cores K7.1 and K7.2 are the same as in Figs. 3 and 5. Ambiguous correlations are labelled with a question mark.

Tables

Table 1: Sample thickness (resolution) of each indicator for cores K6.2, K7.1 and K7.2 from Lake Sapanca, Turkey.

Indicator	Core	Sample thickness
Magnetic susceptibility	All cores	0.1 cm - non destructive
Core description	All cores	Continuous
^{210}Pb / ^{137}Cs	K6.2 and 7.2	1.00 cm
		1.00 cm
Water content	K6.2	1.00 cm
	K7.2	0.25 cm
Grain size (Thin-sections)	K7.1	overlapping 10 cm thin-sections
Grain size (Particle-size analysis)	K7.1; from 0 cm to 10 cm,	0.25 cm
	K7.2; from 10 cm to 34 cm,	0.25 cm
Carbon (TOC/TC/TIC)	K7.2	0.25 cm
Micro-XRF	K7.1	0.05 cm - non destructive
Diatoms	K7.1	0.25 cm
Pollen concentration	K7.1	0.25 cm

Table 2: Summary of disturbance events.*

	Core	Event 1	Event 2	Event 3	Event 4
Core depth [cm]	K6.2	3.25-2.0	-	14.6-10.75	29.0-25.5
	K7.1	6.2-2.25	12.25-8.25	28.0-16.0	37.5-32.5
	K7.2	~6.2-~2.2	~12.7-~8.3	~29-~16.5	-
Sedimentology	K6.2	T_1	-	R	T_4/R?
	K7.1	T_1	H	$T_2/R_1/T_3/R_2$	T_4
	K7.2	T_1	H	$T_2/R_1/T_3/R_2$	-
Indicators		lithology, grain size, diatoms	lithology, grain size	lithology, grain size	lithology, grain size
Interpretation		fast sedimentation, low autochthonous input	material from suspension	T_2andT3: fast sedimentation R_1andR_2: shallow waters, allochthonous material	fast sedimentation
Indicators			magnetic susceptibility, TC	R_1: magnetic susceptibility, Fe	
Interpretation			homogenous sediment	R_1: allochthonous material input, lake wide event	
Indicators		Al, Si, K, Ti		T_2andT3: Al, Si, K, Ti	Al, Si, K, Ti
Interpretation		allochthonous clastic input		T_2andT3: allochthonous clastic input	allochthonous clastic input
Indicators				R_1: Ca, shells, TC	
Interpretation				R_1: shallow water sediments	
Indicator				pollen	pollen
Interpretation				soil input	soil input
^{137}Cs age	K6.2	>1986	-	1963-1986	<1963
	K7.2	>1986	>1986	1963-1986	-
Interpretation		EQ 1999	?	EQ 1967	EQ 1957

*R = reworked facies, T = turbidite-like facies, H = homogeneous facies, EQ = earthquake.

Fig 1

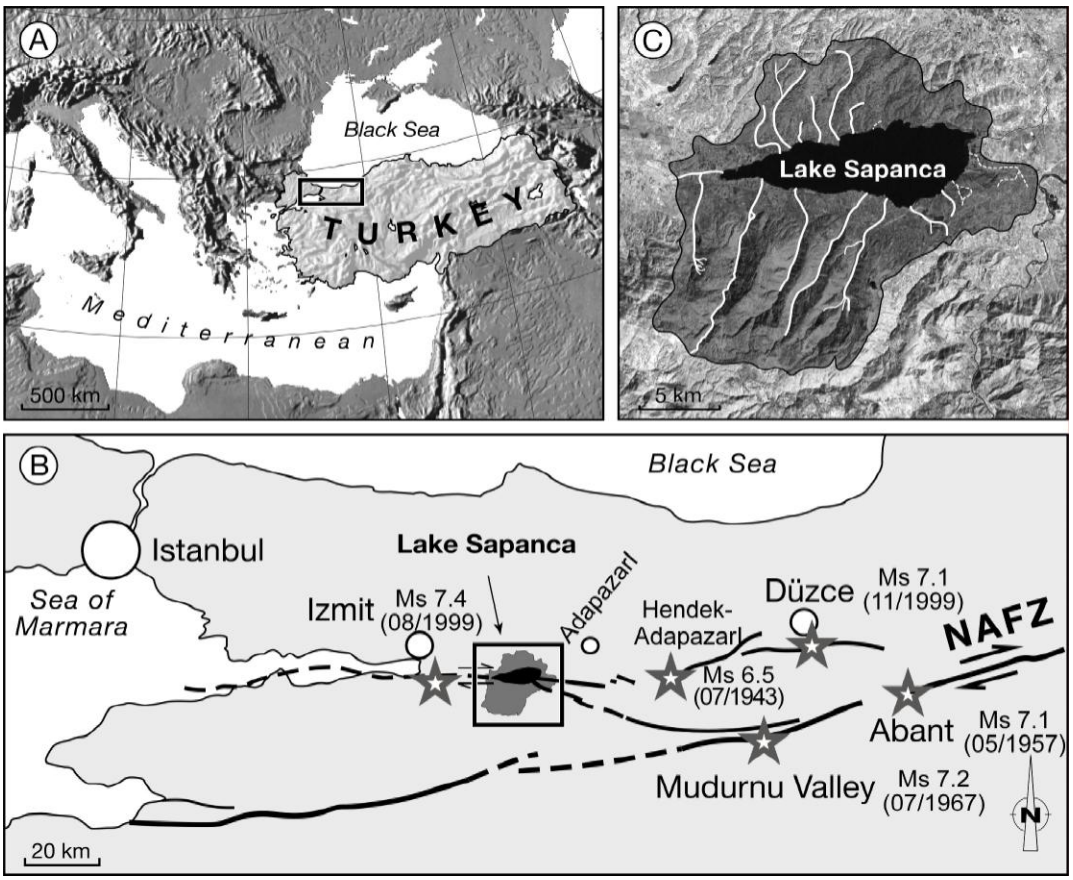
A
Black Sea
TURKEY
Mediterranean
500 km
C
Lake Sapanca
5 km
B
Black Sea
Istanbul
Lake Sapanca
Sea of Marmara
Izmit
Ms 7.4 (08/1999)
Adapazarı
Hendek-Adapazarı
Düzce
Ms 7.1 (11/1999)
NAFZ
Ms 6.5 (07/1943)
Abant
Ms 7.1 (05/1957)
Mudurnu Valley
Ms 7.2 (07/1967)
N
20 km

Fig 2

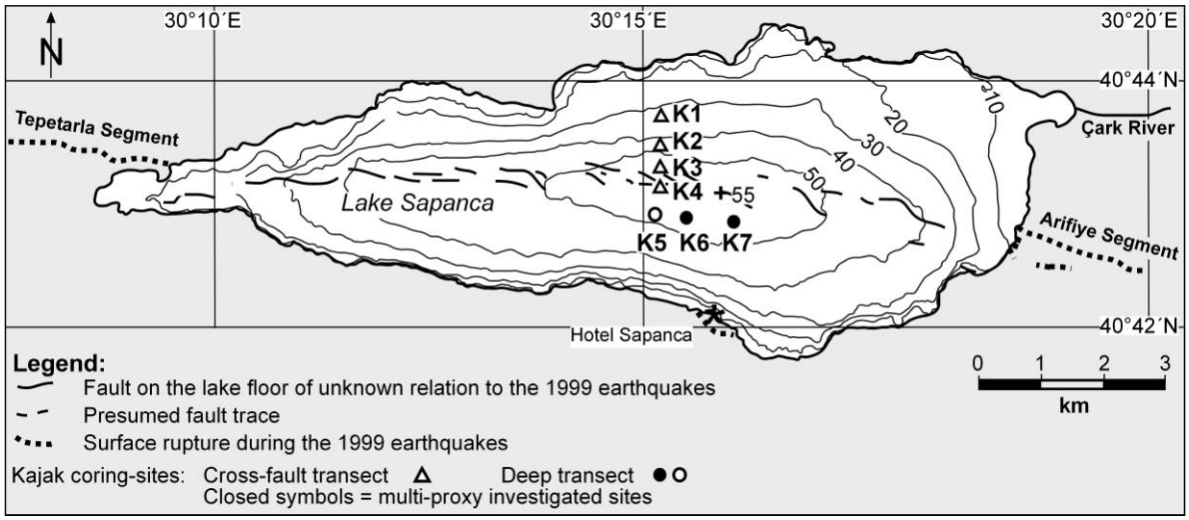
N
30°10´E
30°15´E
30°20´E
40°44´N
40°42´N
Tepetarla Segment
Çark River
Arifiye Segment
Lake Sapanca
Hotel Sapanca
K1
K2
K3
K4
K5
K6
K7
10
20
30
40
50
55
0 1 2 3
km
Legend:
Fault on the lake floor of unknown relation to the 1999 earthquakes
Presumed fault trace
Surface rupture during the 1999 earthquakes
Kajak coring-sites: Cross-fault transect Deep transect
Closed symbols = multi-proxy investigated sites

Fig 3

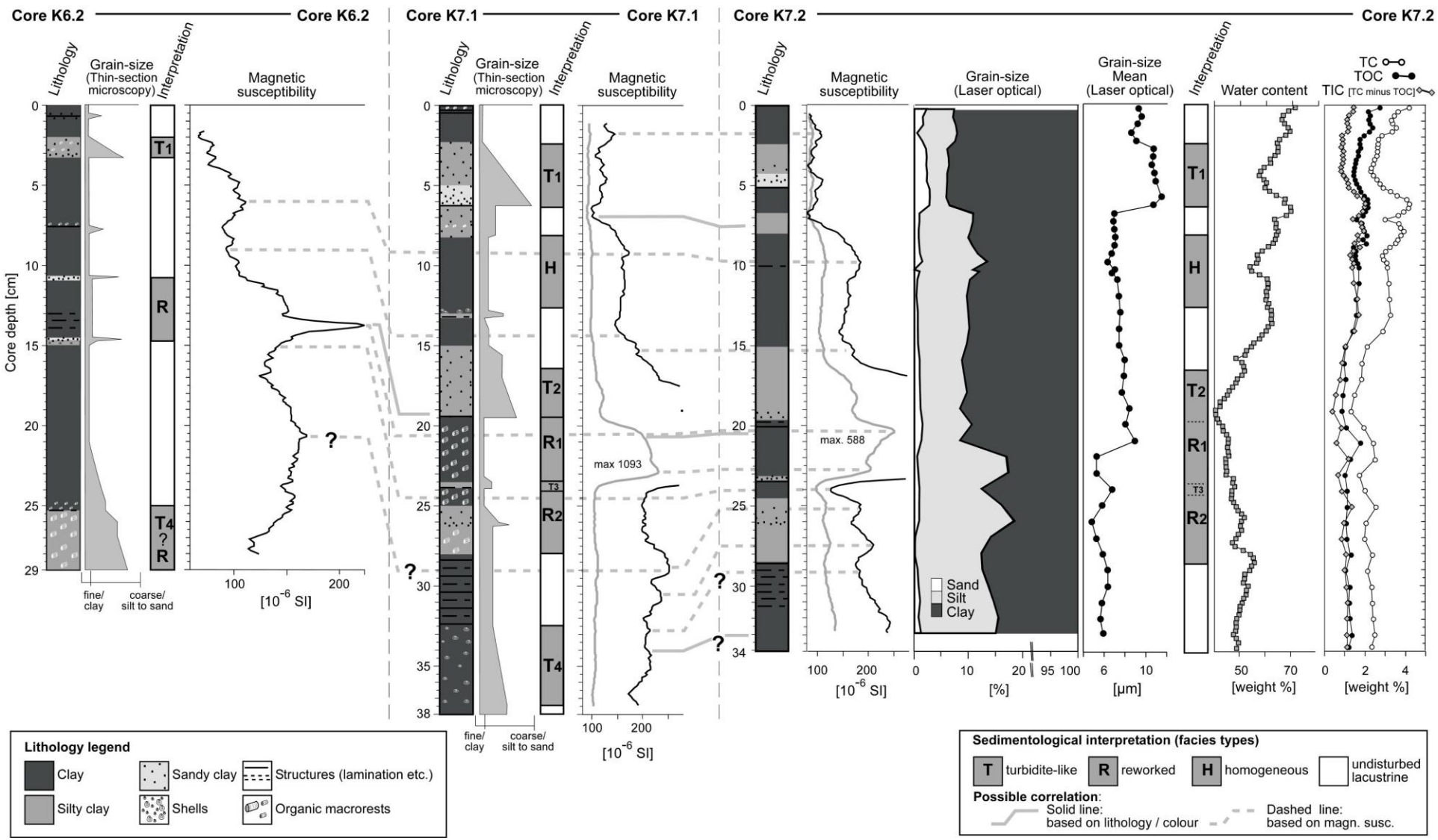
Core K6.2
Core K6.2
Core K7.1
Core K7.1
Core K7.2
Core K7.2
Lithology
Grain-size (Thin-section microscopy)
Interpretation
Magnetic susceptibility
Grain-size (Laser optical)
Grain-size Mean (Laser optical)
Water content
TC
TOC
TIC [TC minus TOC]
Core depth [cm]
T1
R
T4 ? R
H
T2
R1
T3
R2
T4
max 1093
max. 588
Sand
Silt
Clay
fine/ clay
coarse/ silt to sand
[10-6 SI]
[%]
[µm]
[weight %]
Lithology legend
Clay
Silty clay
Sandy clay
Shells
Structures (lamination etc.)
Organic macrorests
Sedimentological interpretation (facies types)
T turbidite-like
R reworked
H homogeneous
undisturbed lacustrine
Possible correlation:
Solid line: based on lithology / colour
Dashed line: based on magn. susc.

Fig 4

Text Fig 4 still in progress!

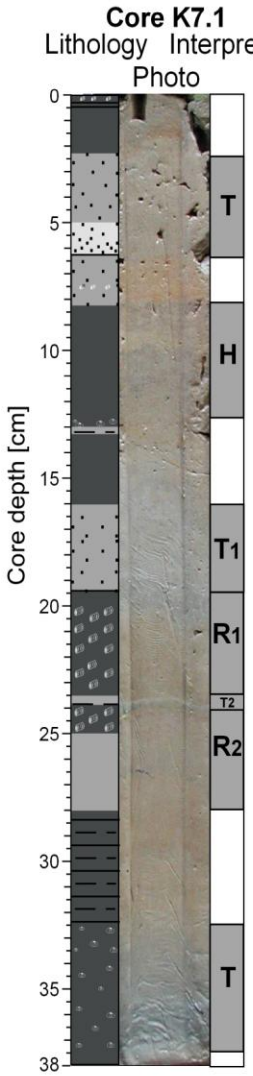

Surface-2.25 cm: 5Y 2.5/1 (olive-red-brown), diatom-rich clay with medium rounded silty and sandy quartz grains; slight laminated from 1 to 0 cm
Undisturbed lacustrine sediment (U-facies)

2.25-6.2 cm: 2.5YR 2.5/0 (reddish-olive-grey), clayed silt with a relatively sharp base and slightly decreasing sand content (quartz) upward
Fining-upward sequence, turbidite-like (T-facies)

6.2-8.25 cm: 5Y 2R/0 (red-brown), diatom-rich silty clay with some organic remains, some well rounded sand and silt grains
U-facies

8.25-12.25 cm: Reddish-olive-grey-brown, homogenous silty clay with some well rounded silty siderite and quartz grains
Homogeneous sequence (H-facies)

12.25-16.0 cm: Reddish-grey-brown, clayish silt with diatoms, well rounded fine silty grain layers (siderite, quartz); from 13-12.75 cm many shell fragments
U-facies

16.0-19.5 cm: Grey clayish silt with a relatively sharp basis and slightly decreasing sandy grain content (quartz, upward), partly angular grains
fining upward sequence, T-facies

19.5-23.25 cm: Reddish-grey-brown, relatively monotonous clayish silt with organic macro-rests (plant remains), broken shell fragments
Reworked sediment sequence (R-facies)

23.25-23.8 cm: Grey clayish silt with a relatively sharp basis and slightly decreasing sandy grain content (quartz, upward), partly angular grains
fining upward sequence, T-facies

23.8-28.0 cm: Reddish-grey-brown, relatively monotonous clayish silt with organic macro-rests (plant remains), 21-26 cm some coarse silty - fine sandy quartz grains, partly broken shell fragments
R-facies

28.0-32.5 cm: Olive-red-brown, partly slightly-laminated, relative homogeneous silty clay
U-facies

32.5-37.5 cm: Grey to light grey, silty clay with a relatively sharp basis and decrease of angular quartz grains; some broken shell fragments
fining upward sequence, T-facies

37.5-38.0 cm: Olive-red-brown, massive clay with well rounded fine-silt-grains, no structures
U-facies

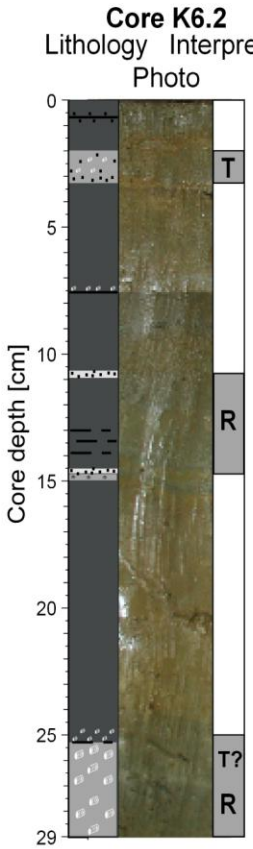

Surface-2.0 cm: Olive-red-brown, diatom-rich clay with medium to non rounded rounded silty and sandy grains; slight lamination at 0.2 cm
Interpretation: Undisturbed lacustrine sediment (U-facies)

2.0-3.25 cm: Reddish-olive-grey, clayish silt with a relatively sharp basis and slightly decreasing sandy grain content (quartz, upward)
fining upward sequence, T-facies

3.25-4.0 cm: Olive-red-brown, diatom-rich silty clay with some organic remains, some well rounded sand and silt grains, slight lamination
U-facies

4.0-10.75 cm: Reddish-olive-grey-brown, clayish silt with diatoms, well rounded fine silty grain layers (siderite, quartz); at 7.0 cm some shell fragments and slight lamination with some well rounded fine sandy quartz grains
U-facies

10.75-14.6 cm: Reddish-grey-brown, relatively monotonous clayish silt with organic macro-rests (plant remains) and small shell remains
Reworked sediment sequence, R-facies

at 14.6 cm: 2 mm thick reddish-grey-brown sandy silt layer, unsorted and mostly angular quartz grains, no graduation
Undisturbed lacustrine sediment / reworked (?)

14.8-25.5 cm: Reddish-olive-grey-brown, clayish silt with diatoms, well rounded fine silty grain layers (siderite, quartz); from 25.5 to 21 cm upward slightly decreasing content of well rounded fine sandy to silty quartz grains
U-facies

25.5-27.5 cm: Olive-grey-brown clayish silt with a weak basis and slightly decreasing sandy grain content (quartz, upward), partly angular grains
R-facies, T-facies (?)

27.5-29.0 cm: Olive-grey-brown, relatively monotonous clayish silt with organic macro-rests (plant remains)
R-facies

Fig 5

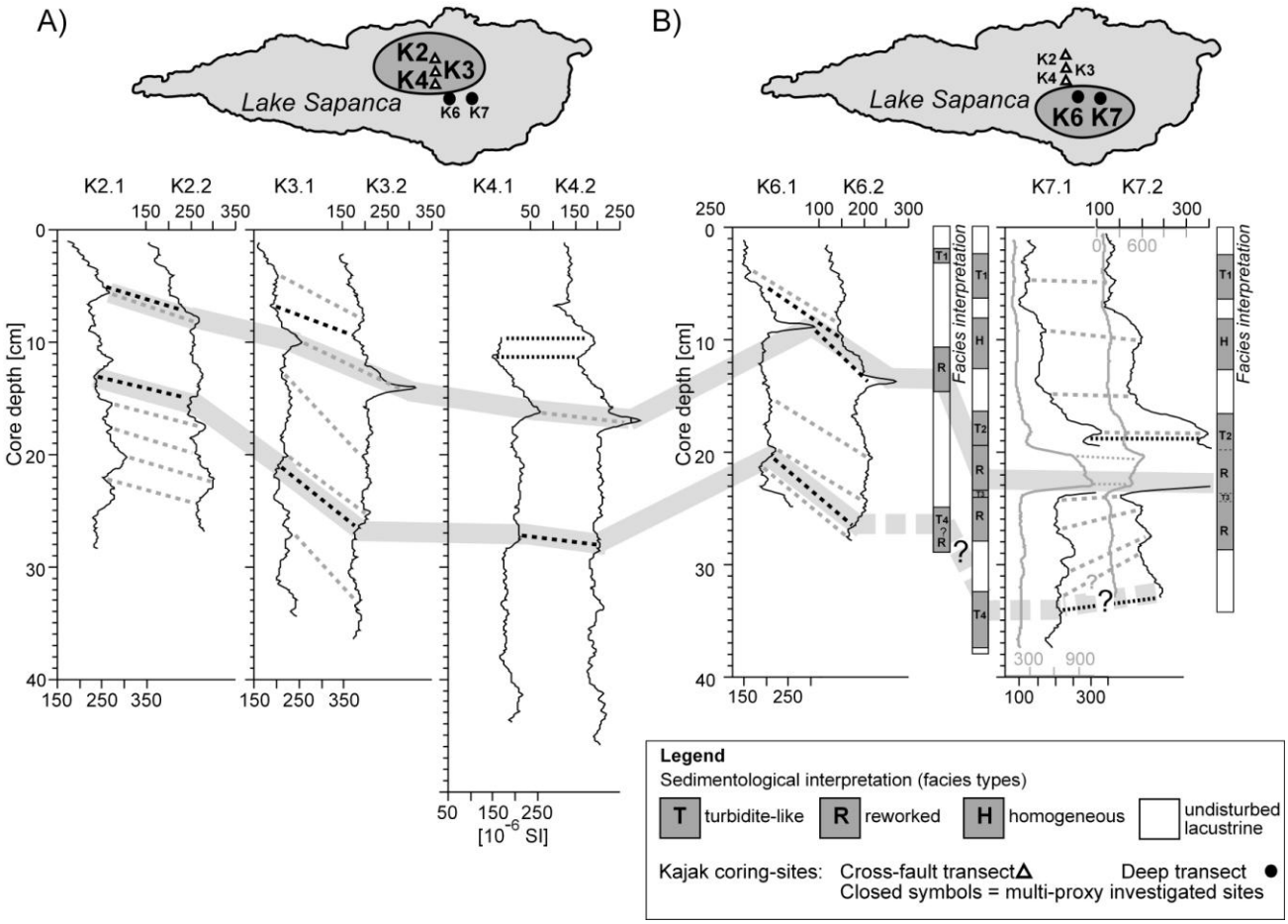
A)
Lake Sapanca
K2
K3
K4
K6
K7
K2.1
K2.2
K3.1
K3.2
K4.1
K4.2
Core depth [cm]
[10⁻⁶ SI]
B)
Lake Sapanca
K6.1
K6.2
K7.1
K7.2
Facies interpretation
T1
H
T2
R
T4
Legend
Sedimentological interpretation (facies types)
T turbidite-like
R reworked
H homogeneous
undisturbed lacustrine
Kajak coring-sites: Cross-fault transect Δ
Deep transect ●
Closed symbols = multi-proxy investigated sites

Fig 6

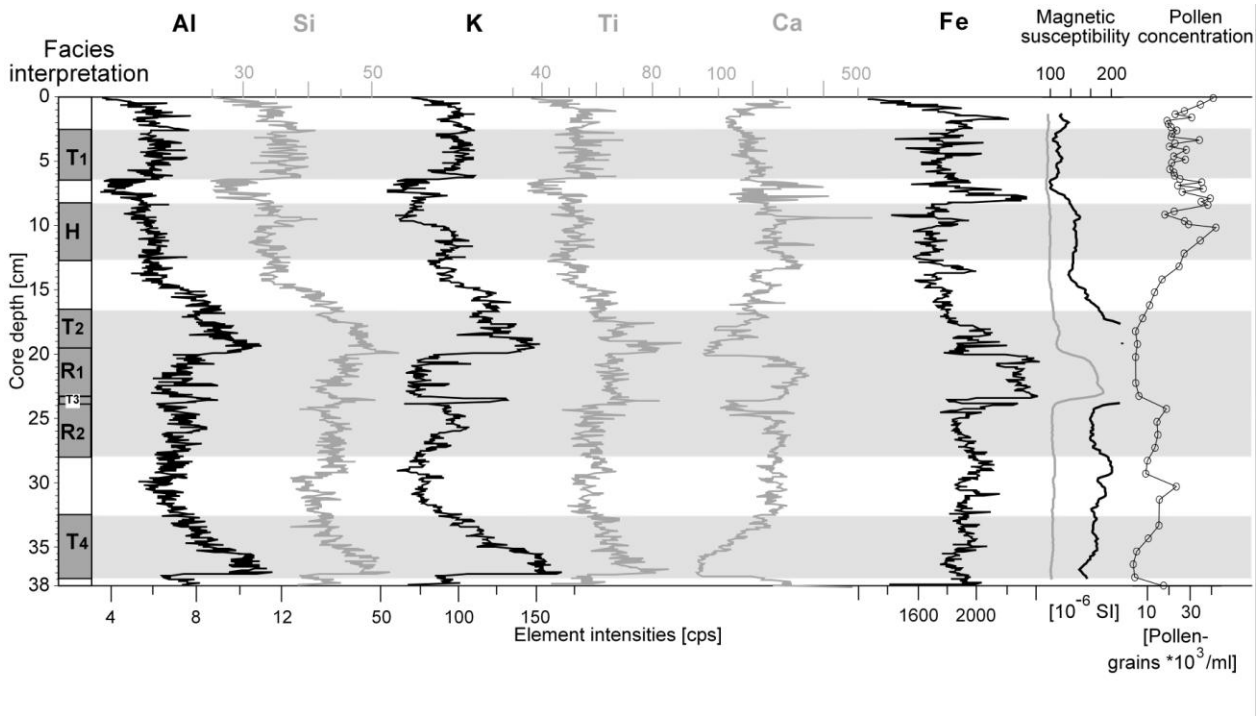
Al
Si
K
Ti
Ca
Fe
Magnetic susceptibility
Pollen concentration
Facies interpretation
Core depth [cm]
T1
H
T2
R1
T3
R2
T4
Element intensities [cps]
[10-6 SI]
[Pollen-grains *10^3/ml]

Fig 7

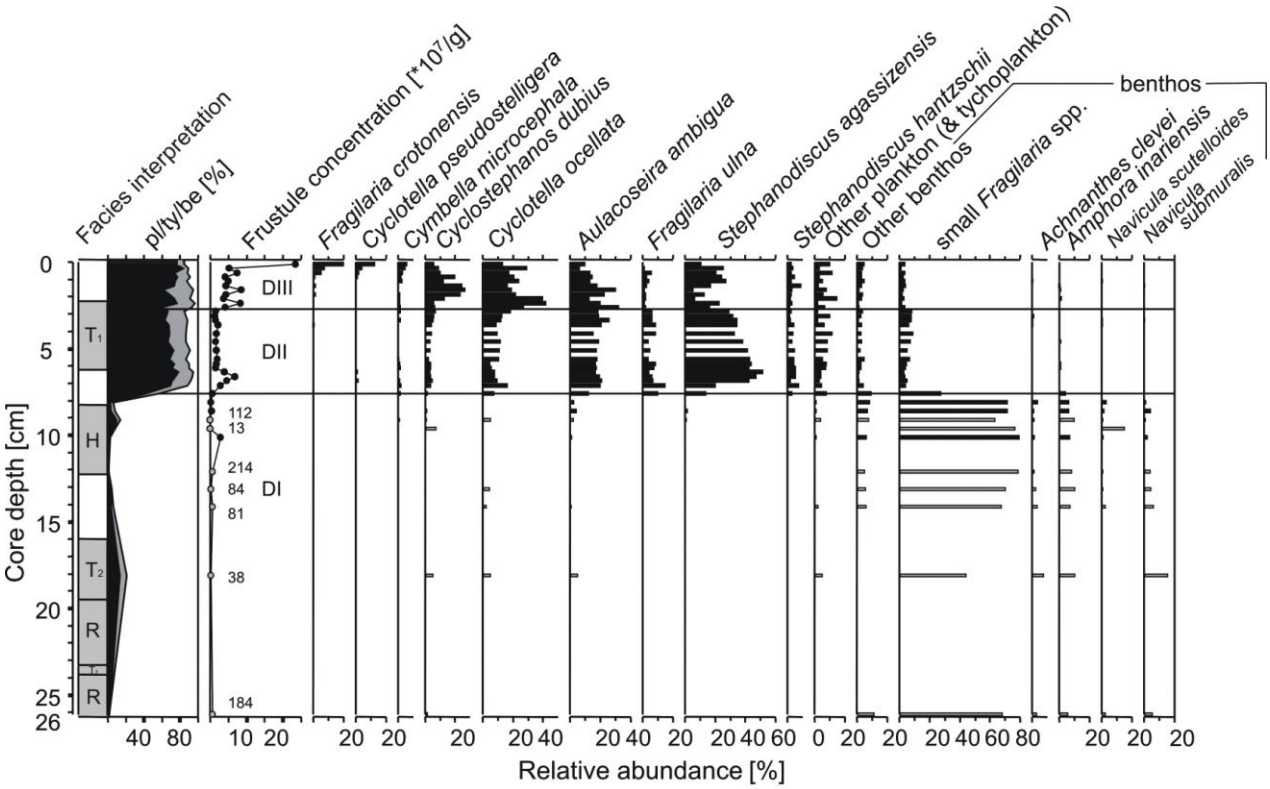
Facies interpretation
pl/ty/be [%]
Frustule concentration [*10⁷/g]
Fragilaria crotonensis
Cyclotella pseudostelligera
Cymbella microcephala
Cyclostephanos dubius
Cyclotella ocellata
Aulacoseira ambigua
Fragilaria ulna
Stephanodiscus agassizensis
Stephanodiscus hantzschii
Other plankton (& tychoplankton)
Other benthos
small Fragilaria spp.
benthos
Achnanthes clevei
Amphora inariensis
Navicula scutelloides
Navicula submuralis
DIII
DII
DI
T1
H
T2
R
R
112
13
214
84
81
38
184
Core depth [cm]
Relative abundance [%]

Fig 8

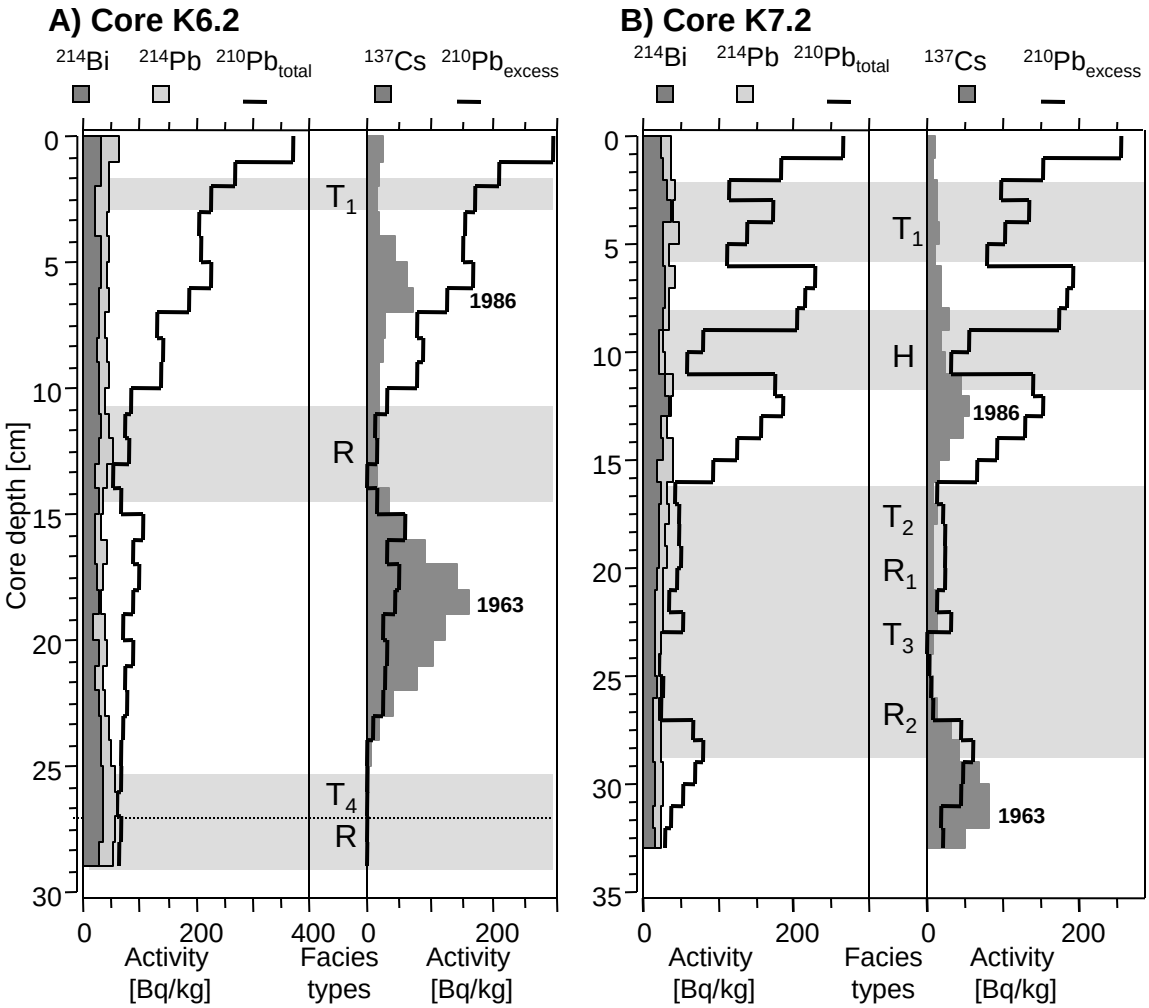
A) Core K6.2
B) Core K7.2
214Bi
214Pb
210Pbtotal
137Cs
210Pbexcess
Core depth [cm]
T1
R
T4
H
T2
R1
T3
R2
1986
1963
Activity [Bq/kg]
Facies types

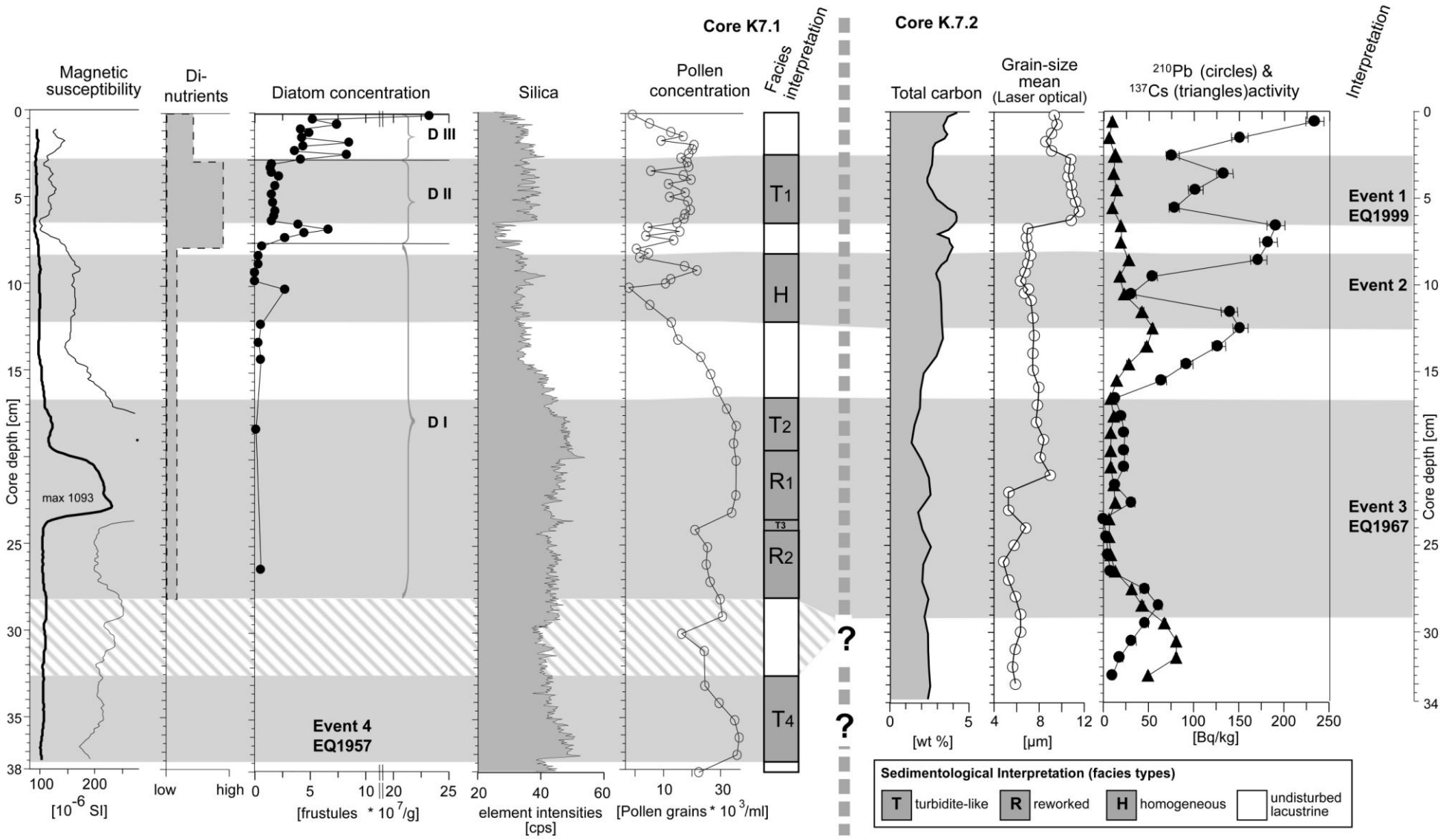
Core K7.1
Core K.7.2
Magnetic susceptibility
Di-nutrients
Diatom concentration
Silica
Pollen concentration
Facies interpretation
Total carbon
Grain-size mean (Laser optical)
210Pb (circles) & 137Cs (triangles)activity
Interpretation
Core depth [cm]
max 1093
D III
D II
D I
T1
H
T2
R1
T3
R2
T4
Event 1 EQ1999
Event 2
Event 3 EQ1967
Event 4 EQ1957
[10-6 SI]
low
high
[frustules * 10 7/g]
element intensities [cps]
[Pollen grains * 10 3/ml]
[wt %]
[µm]
[Bq/kg]
Sedimentological Interpretation (facies types)
T turbidite-like
R reworked
H homogeneous
undisturbed lacustrine

Fig 9